J Solid State Electrochem (2008) 12:1367–1391
DOI 10.1007/s10008-008-0611-6

REVIEW

Electrode materials and reaction mechanisms in solid oxide fuel cells: a brief review

II. Electrochemical behavior vs. materials science aspects

Ekaterina V. Tsipis · Vladislav V. Kharton

Received: 14 April 2008 / Revised: 2 June 2008 / Accepted: 3 June 2008 / Published online: 11 July 2008

Abstract Following previous surveys of the solid electrolyte ceramics and electrode reaction mechanisms in solid oxide fuel cells, this review is focused on the comparative analysis of electrochemical performance, thermal expansion, oxygen ionic and electronic transport, and durability-determining factors in the major groups of electrode materials. The properties of mixed-conducting oxide phases with perovskite-related and fluorite structures, ceramic–metal and oxide composites, and catalytically active additives are briefly discussed, with emphasis on the approaches and findings reported during the last 10–15 years. The performance of conventional and alternative electrode materials in the cells with ZrO_2-, CeO_2-, $LaGaO_3$-, and $La_{10}Si_6O_{27}$-based electrolytes is appraised in the context of potential optimization strategies. Particular attention is centered on the cathode and anode compositions providing maximum electrochemical activity and stability and on the critical aspects relevant for electrode microstructure engineering.

Keywords Oxide electrode · Mixed conductor · Cermet · Intermediate-temperature SOFCs · Surface modification · Thermal expansion · Microstructural degradation

Introduction

Electrical power generation systems based on solid oxide fuel cells (SOFCs) provide important advantages with respect to other energy conversion engines due to high efficiency, fuel flexibility including the prospects to operate on natural gas and biogas, environmental safety, and possibility to recover exhaust heat [1–9]. Significant efforts are, however, still necessary to develop commercially feasible generators, in particular to increase their long-term stability and to reduce costs. These problems can be partially solved by decreasing the SOFC operation temperatures down to 770–1070 K, provided that a high power density and sufficient durability can be achieved in this intermediate-temperature (IT) range. Developments of the IT SOFCs make it possible to use less expensive construction materials, to suppress degradation caused by the high operating temperatures and by thermal cycling, to facilitate miniaturization, and to improve efficiency of the kW-scale generators [2–5, 8–12]. On the other hand, lowering the SOFC operation temperature leads also to a greater role of electrode polarization which may become critical for the overall performance because the apparent activation energies for the interfacial processes are, as a rule, higher than those for oxygen ionic transport in solid electrolytes (e.g., [3–5, 13–19]). The progress in this field is, hence, inevitably associated with a continuous search for novel cathode and anode materials having superior electrocatalytic activity in the intermediate-temperature range, optimization of the cell fabrication technologies and electrode microstructures, and efforts to thoroughly understand the electrochemical reaction mechanisms. These developments have also a key importance for other solid-state electrochemical devices, such as electrolyzers of carbon dioxide and water vapor, oxygen and hydrogen pumps, various ceramic reactors, and sensors [1, 4, 18–21].

This brief review is centered on the analysis of electrochemical behavior, thermal expansion, stability, and oxygen ionic and electronic transport properties in the major groups of SOFC electrode compositions, with primary emphasis on the relationships between electrochemical performance and materials science-related factors. Attention is also drawn to surface

E. V. Tsipis · V. V. Kharton (✉)
Department of Ceramics and Glass Engineering, CICECO,
University of Aveiro,
3810-193 Aveiro, Portugal
e-mail: kharton@ua.pt

modification of the cell components, degradation phenomena, and interaction between electrodes and solid electrolytes. In this paper, no attempt for a complete overview of all promising materials, relevant phase equilibria, and microstructural design approaches, or for a deep analysis of microscopic mechanisms of the electrochemical reactions was made. The readers interested in these issues are addressed to thorough reviews and monographs [1–6, 8–11, 16, 17–29]. Taking into account the data on oxygen ionic conductivity, electrolytic domain boundaries, and thermodynamic stability of solid electrolyte materials discussed in the first part of this review and in [1, 4, 18–20, 30], the data on electrode behavior analyzed in the present work were limited primarily to the electrochemical cells with ZrO_2-, CeO_2-, $LaGaO_3$-, and $La_{10}Si_6O_{27}$-based electrolytes, which can find practical application in SOFCs. The use of other known electrolytes under the SOFC operation conditions is still questionable, mainly due to either poor stability or insufficient ionic transport. Furthermore, the references included in this article were selected in order to show typical relationships between properties of different electrode materials rather than to provide a comprehensive literature survey; priority has been given to the last 10–15 years.

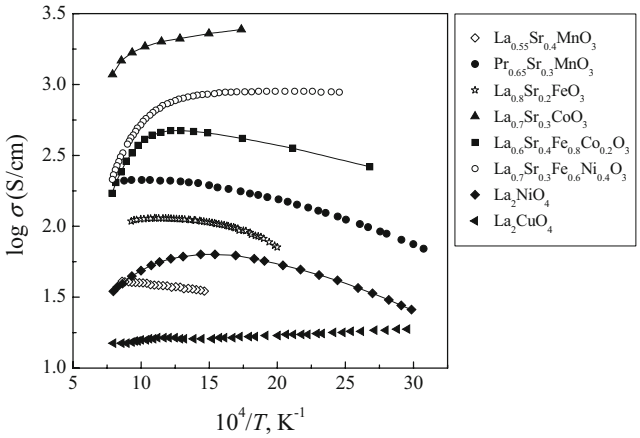

Fig. 1 Comparison of the total conductivity of various perovskite-related materials in air [37, 107, 109, 136, 154, 188, 369]

Cathode materials

Manganites

Perovskite-type manganites $(Ln, A)MnO_{3\pm\delta}$ (Ln = La–Yb or Y; A = Ca, Sr, Ba, Pb) and their derivatives possess a high electronic conductivity, substantial electrocatalytic activity towards oxygen reduction at temperatures above 1000–1100 K, and moderate thermal expansion coefficients (TECs) compatible with commonly used solid electrolytes, such as yttria-stabilized zirconia (YSZ) [1–5, 23, 30]. Although the total conductivity of manganites is lower compared to their Co- and Ni-containing analogues (Fig. 1), the latter perovskite families exhibit other important disadvantages, including excessively high TECs and/or limited thermodynamic stability even under oxidizing conditions. In fact, lanthanum–strontium manganites (LSM) and composites on their basis are still considered as state-of-the-art cathode materials for SOFCs operating at 1070–1270 K [2–9, 26, 31].

Perovskite-like $LnMnO_{3\pm\delta}$ phases exist in all ternary Ln–Mn–O systems, except for Ln = Ce [23, 25]. Ilmenite-type $LnMn_2O_5$ have a considerably lower stability; in air, these are formed up to approximately 1370 K for Ln = Nd–Ho, and up to 1270 K for Ln=Er–Lu and Y. The solubility limits of Ca, Sr, Ba, and Pb in the perovskite lattice of $Ln_{1-x}A_xMnO_{3-\delta}$ (Ln = La–Gd) correspond to the x values varying from 0.4 to 0.7 [23, 25, 32–34]. In the systems with small Ln^{3+} cations such as Yb^{3+} and Y^{3+}, the solubility of Sr^{2+} also achieves at least 40% [25, 35]. At atmospheric oxygen pressure, $p(O_2)$, $Ce_{1-x}Sr_xMnO_{3-\delta}$ with tetragonal perovskite structure are formed in the range x=0.7–0.9 [36]. When the content of alkaline-earth dopants in $Ln_{1-x}A_xMnO_{3-\delta}$ is modest (<20%), minor Ln-site cation deficiency increases thermodynamic stability, while rare-earth oxides may segregate in the nominally cation-stoichiometric compositions [25, 37, 38]. Most of K_2NiF_4-type $(Ln, A)_2MnO_{4\pm\delta}$ exist at moderately lower oxygen pressures with respect to atmospheric, except for the compounds with comparable Ln^{3+} and A^{2+} concentrations which may be obtained in air [23, 25, 39].

All perovskite-related manganites exhibit a predominant electronic conduction in combination with low oxygen ion diffusivity; their transport properties and electrochemical activity are strongly dependent on the oxygen non-stoichiometry. In particular, the electrocatalytic behavior under high cathodic polarization is usually correlated with oxygen vacancy generation at the electrode surface [26, 29, 40, 41]. At atmospheric $p(O_2)$ and temperatures below 1273 K, $La_{1-x}Sr_xMnO_{3\pm\delta}$ phases are oxygen-hyperstoichiometric at $x\leq0.2$ and become deficient on further doping [25, 42]. The electrical conductivity (σ) of $Ln_{1-x}A_xMnO_{3\pm\delta}$ at moderate A^{2+} concentrations increases with x as Mn^{4+} fraction increases; typical trends are illustrated by Figs. 2b and 3b. The conductivity maximum lies in the range x=0.2–0.5 and shifts towards lower dopant content on heating. In the case of $Ln_{0.7}Sr_{0.3}MnO_{3\pm\delta}$ (Ln = La–Gd) series, the highest conductivity was reported for $Nd_{0.7}Sr_{0.3}MnO_{3\pm\delta}$ above 760 K and for $Pr_{0.7}Sr_{0.3}MnO_{3\pm\delta}$ at lower temperatures [43]. A summary on the average TECs of manganite ceramics is presented in Table 1. Decreasing rare-earth cation radii in $Ln_{1-x}A_xMnO_{3\pm\delta}$ at fixed A^{2+} concentration suppresses the lattice expansion on heating. The dopant contents corresponding to an optimum thermomechanical compatibility with zirconia solid electrolytes increase from x=0.10–

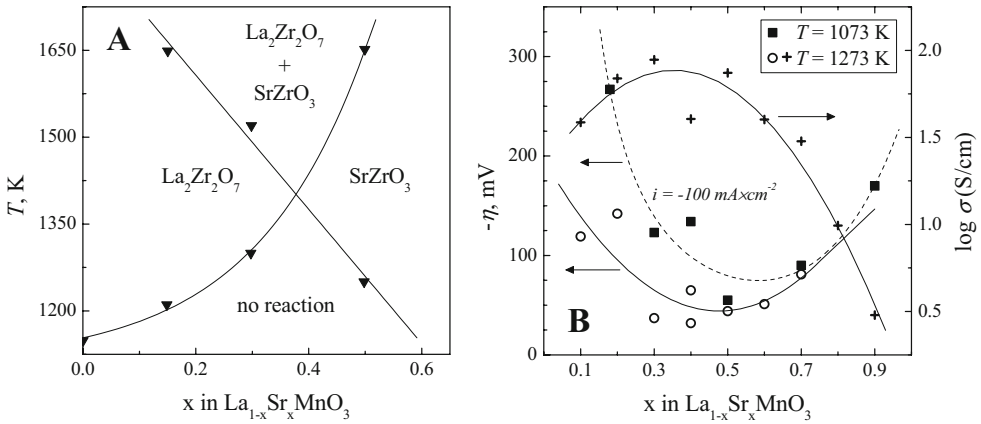

Fig. 2 Approximate temperature limits which correspond to starting extensive interaction between $La_{1-x}Sr_xMnO_3$ and ZrO_2, leading to $La_2Zr_2O_7$ or $SrZrO_3$ formation [47] (**a**), and cathodic overpotentials [34, 35, 51, 111] and total conductivity [34] of $La_{1-x}Sr_xMnO_3$ in air (**b**). All polarization data correspond to zirconia-based solid electrolytes. The overpotentials at 1073 K are shown for x=0.18 [111], 0.3 [51], 0.4 [35], and 0.5–0.9 [51]. At 1273 K, these values are given for x=0.1–0.7 [34] and for x=0.4 [35]

0.15 (Ln = La) up to x=0.3–0.5 for Gd-containing materials [43].

Acceptor-type doping leads to a substantial improvement in the performance of porous $Ln_{1-x}A_xMnO_{3\pm\delta}$ cathodes (Figs. 2, 3 and 4). The maximum of electrochemical activity at 1073–1273 K observed in the range x=0.3–0.7 tends to shift towards lower dopant concentrations when temperature increases and is close enough to the conductivity maximum. Introducing Ln-site cation deficiency increases the manganite electrode performance due to a suppressed reactivity with zirconia electrolytes, higher oxygen vacancy content and, often, faster ionic conduction [25, 37, 38, 44, 45]. In addition, this compositional variable makes it possible to optimize thermal expansion (Table 1). The common cathode compositions are based on $(La_{1-x}Sr_x)_{1-y}MnO_{3\pm\delta}$ with x= 0.10–0.30 and y=0.05–0.12, although in many cases the electrochemical activity of $PrMnO_3$-based materials is higher (Fig. 4). The superior properties of praseodymium-containing solid solutions, such as $Pr_{0.6}Sr_{0.4}MnO_{3-\delta}$ [35] and $Pr_{0.7}Ca_{0.3}MnO_{3-\delta}$ [46], may be associated with a non-negligible contribution of $Pr^{3+/4+}$ redox couple at the electrode surface and with a less pronounced interaction with zirconia during cell processing and operation. The latter factor has a critical importance for most $Ln_{1-x}A_xMnO_{3\pm\delta}$ cathodes [1, 13, 25, 26, 32, 34, 47–50], since the resultant formation of $AZrO_3$-based perovskite and $Ln_2Zr_2O_7$ pyrochlore layers increases ohmic losses owing to very low conductivity of the reaction products and leads to a high polarization due to blocking of oxygen transfer. For Ln = La–Gd, the reactivity with YSZ to form $Ln_2Zr_2O_7$ becomes lower on decreasing Ln^{3+} radius [35, 43, 47, 51]; this originates from decreasing thermodynamic stability of the pyrochlore zirconates compared to their fluorite-like polymorphs. At the same time, reducing the Ln^{3+} size and perovskite tolerance factor decreases also stability of the manganite solid solutions [52], which may facilitate the cell materials interaction. This complex behavior in combination with various microstructure-related effects leads often to

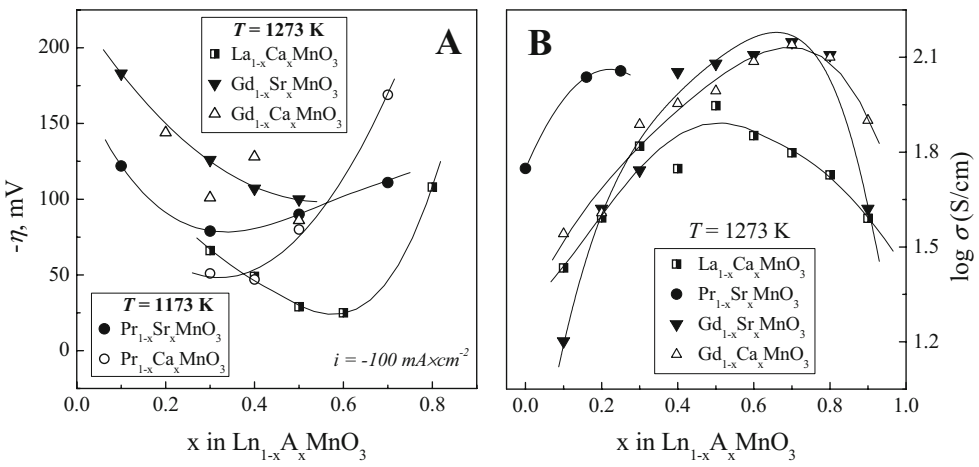

Fig. 3 Composition dependencies of the cathodic overpotentials in contact with YSZ (**a**) and total conductivity (**b**) of selected $Ln_{1-x}A_xMnO_3$ solid solutions in air [33–35, 46, 362]

Table 1 Average linear TECs of manganite ceramics in air [32, 35, 43–46, 90, 306, 362–364]

Composition	*T*, K	$\overline{\alpha} \times 10^6$, K^{-1}
$La_{0.99}MnO_3$	300–1370	11.2
$La_{0.94}Sr_{0.05}MnO_3$	300–1370	11.7
$La_{0.89}Sr_{0.10}MnO_3$	300–1370	12.0
$La_{0.79}Sr_{0.20}MnO_3$	300–1370	12.4
	300–1270	11.1
$La_{0.69}Sr_{0.30}MnO_3$	300–1370	12.8
$La_{0.65}Sr_{0.30}MnO_3$	300–1270	12.3
$La_{0.69}Sr_{0.30}MnO_3$	300–1270	12.0
$La_{0.50}Sr_{0.40}MnO_3$	300–1100	11.3
$La_{0.50}Sr_{0.30}MnO_3$	300–1100	12.3
$La_{0.30}Sr_{0.50}MnO_3$[a]	300–1100	11.9
$LaMnO_3$	320–580	7.7
	580–1100	11.8
$La_{0.90}Sr_{0.10}MnO_3$	300–1270	9.9
$La_{0.80}Sr_{0.20}MnO_3$	300–1270	11.2
	340–540	7.7
$La_{0.70}Sr_{0.30}MnO_3$	300–1270	11.7
$La_{0.60}Sr_{0.40}MnO_3$	570–1270	13.0
	320–1100	11.7
	300–1100	11.3
	300–1270	12.0
$La_{0.50}Sr_{0.50}MnO_3$	300–1100	12.1
	300–1270	12.2
	320–1100	12.3
$La_{0.80}Ca_{0.20}MnO_3$	320–520	6.3
	550–1050	10.6
$La_{0.60}Ca_{0.40}MnO_3$	350–1050	9.3
$La_{0.50}Ca_{0.50}MnO_3$	350–1050	10.7
$La_{0.60}Pb_{0.40}MnO_3$	550–1100	9.2
$La_{0.50}Pb_{0.50}MnO_3$	300–1100	10.4
$Pr_{0.80}Sr_{0.20}MnO_3$	300–1270	9.6
	300–1270	10.1
$Pr_{0.75}Sr_{0.25}MnO_3$	300–1170	10.2
$Pr_{0.70}Sr_{0.30}MnO_3$	300–1270	10.6
	300–1070	11.1
$Pr_{0.65}Sr_{0.30}MnO_3$	300–1270	11.6
$Pr_{0.60}Sr_{0.40}MnO_3$	570–1270	12.0
	300–1270	11.6
$Pr_{0.50}Sr_{0.50}MnO_3$	300–1270	12.2
$Pr_{0.70}Ca_{0.30}MnO_3$	570–1270	11.9
$Nd_{0.80}Sr_{0.20}MnO_3$	300–1270	9.6
$Nd_{0.75}Sr_{0.25}MnO_3$	300–1170	10.7
$Nd_{0.70}Sr_{0.30}MnO_3$	300–1270	10.3
	300–1070	11.1
$Nd_{0.65}Sr_{0.30}MnO_3$	300–1270	9.7
$Nd_{0.60}Sr_{0.40}MnO_3$	300–1270	11.2
$Nd_{0.50}Sr_{0.50}MnO_3$	300–1270	12.1
$Nd_{0.50}Ca_{0.50}MnO_3$	500–1200	11.3
$Sm_{0.70}Sr_{0.30}MnO_3$	300–1270	9.9
$Sm_{0.60}Sr_{0.40}MnO_3$	300–1270	10.4
$Sm_{0.50}Sr_{0.50}MnO_3$	300–1270	11.4
$Gd_{0.80}Sr_{0.20}MnO_3$	300–1270	3.8
$Gd_{0.70}Sr_{0.30}MnO_3$	300–1270	9.5
$Gd_{0.65}Sr_{0.30}MnO_3$	300–1270	9.9
$Gd_{0.60}Sr_{0.40}MnO_3$	300–1270	10.2
$Gd_{0.50}Sr_{0.50}MnO_3$	300–1270	10.9
$Gd_{0.50}Ca_{0.50}MnO_3$	300–1070	10.0
$Yb_{0.50}Ca_{0.50}MnO_3$	300–1100	10.2
$Y_{0.50}Ca_{0.50}MnO_3$	450–670	3.0
	670–1100	9.1

[a] Manganese oxide phase impurities

contradictions in the literature data, particularly on the role of A^{2+} cation radii [25, 33–35, 43]. In contrast, the positive impact of minor Ln-site cation deficiency inhibiting topotactic reaction was unambiguously established by numerous groups [38, 53–56]. Under the SOFC operating conditions, the zirconate formation can be partly suppressed due to a reduced oxygen activity at the cathode, favorable for dissociation and re-dissolution of the blocking layers [38, 56]. Notice however that reducing $p(O_2)$ may also cause Sr enrichment of the LSM surface [57].

An optimization of thermal expansion, improvement of the interfacial stability and, often, an increase in the oxygen permeability and electrode performance can be achieved by the partial substitution of manganese with other transition-metal cations and/or ions having a stable oxidation state (e.g., [23, 25, 32, 52, 58–60] and references cited). As a general rule, moderate additions of the variable-valence dopants decrease polarization resistance (R_η) of the cathodes made of $(Ln, Sr)(Mn, M)O_{3-\delta}$ (M = Co, Ni) perovskites; the use of cations with constant oxidation state enables to optimize thermal and chemical expansion and, thus, to improve microstructural stability. The effects of Mn-site substitution on the interaction with solid electrolyte materials

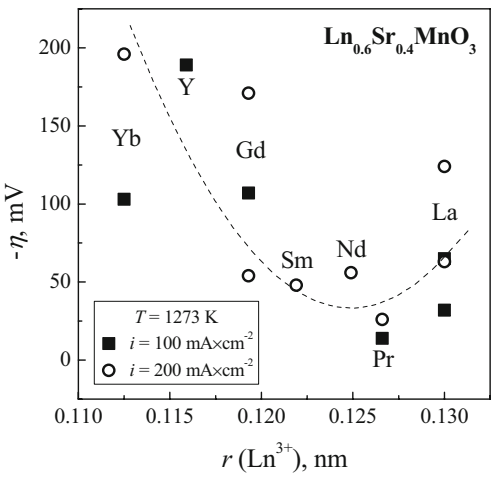

Fig. 4 Cathodic overpotentials of porous $Ln_{0.6}Sr_{0.4}MnO_3$|YSZ electrodes [33–35] as function of the Ln^{3+} cation radius. The radii are given for 8-fold coordination

depend on numerous factors, including the thermodynamic stability of perovskite solid solutions and dopant diffusivity in the electrolyte, as briefly discussed below. Several examples illustrating the performance of doped manganite cathodes are presented in Fig. 5. In most known cases, no direct correlations between the oxygen ionic conductivity (σ_o) in the mixed-conducting electrode materials and electrochemical behavior of the porous cathodes can be unambiguously identified when the dopant content is moderate. These correlations become quite obvious in the composite layers containing a second ionically conducting phase, such as stabilized zirconia or doped ceria [61–66]. A highest electrochemical activity is demonstrated by functionally graded cathodes, where the ionic conductor (IC) volume fraction near the electrode–electrolyte interface is substantial and the nano-sized manganite particles are distributed at the IC surface, thus providing a maximum electrochemical reaction zone. Nonetheless, the overall performance typical for porous manganite-based layers in the IT SOFCs with ceria and lanthanum gallate electrolytes is usually lower compared to ferrite- and cobaltite-based electrodes [14, 26, 67].

Ferrites

The number of iron-containing oxide phases, which are stable under the SOFC cathodic conditions and exhibit a significant electronic or mixed conductivity, is larger than that in the manganite systems. These primarily include perovskite-like $(Ln, A)FeO_{3\pm\delta}$ and their derivatives existing in all Ln–A–Fe–O systems, $A_2Fe_2O_{5\pm\delta}$ brownmillerites, $(Ln, A)_3Fe_5O_{12\pm\delta}$ garnets in the systems with relatively small Ln^{3+} cations, Ruddlesden–Popper series $(Ln,A)_{n+1}Fe_nO_z$, and a variety of other intergrowth compounds such as $Sr_4Fe_6O_{13\pm\delta}$ ([21, 23, 25, 68–81] and references cited). However, due to structural constraints and defect chemistry features limiting electronic transport, in most cases an extensive iron substitution is necessary to achieve the total conductivity values higher than 10–30 S/cm at temperatures above 700 K. For undoped ferrites, the maximum conductivity under cathodic conditions is characteristic of perovskite-related solid solutions, such as $Ln_{1-x}Sr_xFeO_{3-\delta}$ systems where the highest level of electronic and ionic transport is known for Ln = La and $x\approx0.5$ [78–81]. While moderate additions of the acceptor-type cations enhance the concentrations of mobile oxygen vacancies and *p*-type electronic charge carriers in $(Ln, A)FeO_{3-\delta}$, increasing A^{2+} content above 50% and decreasing average cation radius in the Ln^{3+} sites promote vacancy-ordering and hole localization processes with a negative influence on the transport properties. In the Ruddlesden–Popper series, the partial electronic and ionic conductivities tend to decrease when the concentration of rock salt-type $(Ln,A)_2O_2$ layers increases; the general trends observed on acceptor doping are similar to those in the perovskite systems (e.g., [39, 76, 77, 82]). The maximum total conductivity in $La_{2-x}Sr_xFeO_{4\pm\delta}$ phases with K_2NiF_4-type structure, 10–25 S/cm at 670–1270 K, corresponds to $x=1.2$–1.3 [82].

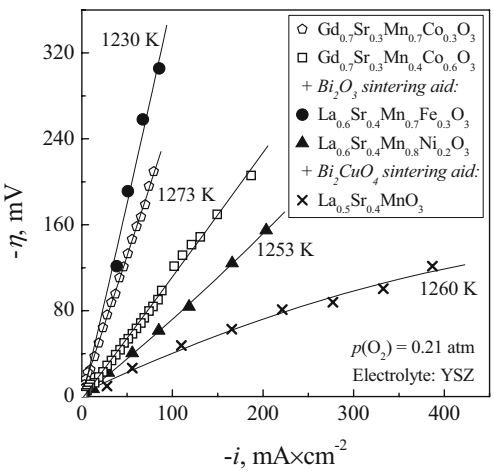

Fig. 5 Cathodic overpotential vs. current density dependencies for several O_2,(Ln,Sr)(Mn,M)O_3|YSZ half cells fabricated with and without sintering aids, in air [25, 50, 59, 181, 357]

If compared to manganite electrode materials, one important disadvantage of perovskite-related ferrites relates to a high chemical expansion, which provides critical contribution to the apparent TECs due to oxygen losses at elevated temperatures and may lead to thermomechanical incompatibility with common solid electrolytes [75, 83–86]. The expansion can be partly suppressed by the partial substitution of iron with cations having a more stable oxidation state, thus reducing oxygen non-stoichiometry variations; the dopant examples include Ga, Al, Ti, and Cr [75, 86–89]. However, this type of doping decreases electronic and, often, ionic transport. The incorporation of nickel increases the conductivity [85, 90–92]; thermal expansion of La(Fe,Ni)O_3-based perovskites remains moderate at temperatures up to 1100–1300 K, but rises on further heating, making it necessary to carefully optimize the electrode sintering protocols. The layered ferrite phases, particularly Ruddlesden–Popper series and brownmillerites, display modest stoichiometry changes and better thermomechanical properties compared to the perovskites, although their compatibility with electrolyte ceramics is still limited [39, 76, 77, 82, 93, 94].

The rate of $La_2Zr_2O_7$ formation due to the reaction of $LaFeO_{3-\delta}$ and YSZ at 1673 K was reported to be much lower in comparison with lanthanum manganite, and can be further reduced by Al^{3+} incorporation [58]. On the contrary, the minimum reactivity between $(La_{0.6}A_{0.4})_{1-x}Fe_{0.8}M_{0.2}O_{3-\delta}$ (A = Sr, Ca; M = Cr, Mn, Co, Ni) and YSZ at 1273 K was found for Mn doping, which promotes however the cubic to monoclinic phase transition of zirconia on long-term testing [95, 96]. As for manganites, minor A-site cation deficiency improves the stability of ferrite-based perovskites in contact with YSZ; opposite effects are observed on Ba^{2+} incorporation and on

decreasing Ln^{3+} cation radius [95–97]. In addition to $Ln_2Zr_2O_7$ pyrochlore and $AZrO_3$ perovskite-like phases, the interaction with zirconia leads usually to the segregation of Fe_2O_3 or spinels, such as $CoFe_2O_4$ [96–99]. The equilibrium phase relationships and interaction mechanisms in the systems comprising $(Ln, A)FeO_{3-\delta}$ and CeO_2- or $LaGaO_3$-based solid electrolytes differ significantly from those for stabilized ZrO_2 [87, 100–105]. The pseudobinary $(Ln, A)(Fe, M)O_{3-\delta} - (La, A)(Ga, Mg)O_{3-\delta}$ systems are all characterized with large solid solution domains, facilitating cation interdiffusion between the phases. In the case of ceria, the interaction occurs primarily via Ln^{3+} dissolution in the fluorite-type $Ce(Ln)O_{2-\delta}$ and grain-boundary diffusion of transition metal cations, such as iron. Consequently, the rate of materials interaction and its negative impact on the electrochemical properties is minimum in the fuel cells with CeO_2-based components; the introduction of doped ceria buffer layers between oxide cathodes and either zirconia or $La_{1-v}Sr_vGa_{1-w}Mg_wO_{3-\delta}$ (LSGM) electrolytes enables to considerably improve the SOFC performance [99, 106].

Reducing the SOFC operating temperature results in a lower oxygen vacancy concentration and, hence, in a greater role of the electrode material ionic conductivity. The oxygen diffusivity is strongly influenced by the content of lower-valence cations, which should be increased up to possible maximum; however, extensive acceptor doping is usually accompanied with increasing thermal and chemical expansion due to weakening of the metal–oxygen bonds and rising the atomic vibration unharmonicity [86, 107, 108]. One attractive example refers to the well-known $La_{1-x}Sr_xFe_{1-y}Co_y O_{3-\delta}$ (LSFC) system where moderate dopant additions provide a significant enhancement in the total conductivity and electrochemical activity, but also increase apparent TECs (Table 2 and Fig. 6). On the creation of La-site cation vacancies in LSFC, the conductivity and thermal expansion both decrease owing to dominant charge-compensation mechanism via the oxygen vacancy formation [109]; this limits the hole concentration and oxygen non-stoichiometry variations on heating. Similar effects on the electronic transport and TECs are observed in $Ln_{0.8}Sr_{0.2} Fe_{0.8}Co_{0.2}O_{3-\delta}$ (Ln = La–Gd) when the Ln^{3+} size becomes smaller; the latter is also associated with lowering thermodynamic stability and narrowing the perovskite solid-solution domains [110]. An optimum combination of thermomechanical, transport and electrochemical properties in LSFC is characteristic for the compositions with x=0.2–0.5 and $y\approx$0.2, considered as promising cathode materials for the IT SOFCs with ceria-based electrolytes. As an example, the cathodic overpotentials of porous $La_{0.6}Sr_{0.4}Fe_{0.8}Co_{0.2} O_{3-\delta}$ layers in contact with $Ce_{0.8}Sm_{0.2}O_{2-\delta}$ are 10–40 times lower than those of $La_{0.82}Sr_{0.18}Fe_{0.8}MnO_{3-\delta}|YSZ$ at 973–1173 K [111]; this difference increases on reducing temperature. The polarization resistance of $La_{0.6}Sr_{0.4}Fe_{0.8}Co_{0.2} O_{3-\delta}$ double-layer cathode comprising one thick porous layer and a thin dense film, applied onto 10 or 20 mol% gadolinia-doped ceria (CGO), was reported to be as low as 0.5 Ω cm^2 at 793 K [112].

Cobaltites

In comparison with the ferrite-based materials, perovskite-related cobaltites possess considerably better cathodic and transport properties, but also a higher thermal and chemical expansion [21, 25, 26, 39, 107, 113–125]. The latter feature illustrated by Table 2 limits the compatibility with solid oxide electrolytes, mainly to derivatives of δ-Bi_2O_3, $Bi_2VO_{5.5-\delta}$, and $La_2Mo_2O_{9-\delta}$. As for the manganite and ferrite electrodes, the primary attention for potential electrochemical applications is drawn to perovskite-type $(Ln, Sr)CoO_{3-\delta}$ and solid solutions on their base. At the same time, substantially lower TECs, relatively high mixed conductivity and fast exchange kinetics results in a significant interest to the layered cobaltites where the state of Co cations is often more stable with respect to disordered perovskite analogues; important compositional families are $LnBaCo_2O_{5+\delta}$ (Ln = Pr, Gd–Ho, Y), $LnBaCo_4O_{7+\delta}$ (Ln = Dy–Yb, Y), and also Ruddlesden–Popper type $(Ln,A)_4Co_3O_{10}$ and $(Ln, A)_2 CoO_{4\pm\delta}$ (Ln = La–Nd) existing at moderately reduced oxygen pressures ([25, 115, 126–135] and references therein). The information on long-term performance of such materials under the SOFC cathodic conditions is, however, scarce.

Perovskite-like $(Ln, A)CoO_{3-\delta}$ exhibit a greater hole delocalization and mobility with respect to their Mn- and Fe-containing analogues (Table 2, Figs. 1 and 7). At 800–1300 K, the maximum total conductivity in $Ln_{1-x}A_x CoO_{3-\delta}$, predominantly p-type electronic, is observed for Ln = La–Sm, A = Sr, and x=0.25–0.50, shifting towards lower x on heating [25, 115, 136–140]. Introducing Ln-site vacancies leads often to decreasing ionic and electronic transport, although the effects of cation deficiency are governed by particular charge-compensation mechanisms dependent on the Ln/A ratio, temperature, and oxygen pressure; moreover, the corresponding electrical and structural data may be influenced by synthesis conditions, pre-history, and microstructure because the cobaltite perovskites have a lower thermodynamic stability and are less tolerant to the cation non-stoichiometry in comparison with manganites and ferrites [25, 125, 141, 142]. For $La_{2-x}Sr_xCoO_{4\pm\delta}$ (x=0.7–1.0), the total conductivity above 870 K in air becomes comparable to that of K_2NiF_4-type nickelates, 80–100 S/cm [39]. The highest level of oxygen ionic transport in $Ln_{1-x}A_xCoO_{3-\delta}$ corresponds to x=0.65–0.70 and Ln = La [21, 137]. This level is not exceptional, but lies close to maximum known for the oxide mixed conductors where higher oxygen permeability was only reported for Bi_2O_3-containing materials and for perovskite-type phases derived

Table 2 Selected data on the total conductivity and thermal expansion coefficients of $La_{1-x}Sr_xFe_{1-y}Co_yO_{3-\delta}$ ceramics in air

x	Y	Total conductivity, S/cm		Average TECs		Ref.
		873 K	1073 K	T, K	$\overline{\alpha} \times 10^6$, K^{-1}	
0	0.2	0.8	4.5	373–773	13.1	[365]
				873–1173	17.5	[365]
0.1	0.2	44	59	573–1173	16.0	[365]
0.1	1.0	1.27×10^3	1.21×10^3			[136]
0.2	0	93	93	573–1173	12.6	[366]
			1.09×10^2			[154]
0.2	0.1	1.16×10^2	1.23×10^2	473–1173	14.5	[366]
0.2	0.2	1.75×10^2	1.91×10^2	373–1073	15.4	[365]
		1.27×10^2	1.49×10^2	373–1073	15.4	[366]
		77	87	303–1273	14.8	[136]
		1.76×10^2	1.64×10^2	973	12.5	[110]
0.2	0.3	1.87×10^2	2.24×10^2	373–1173	16.5	[366]
0.2	0.4	3.39×10^2	2.87×10^2	373–1173	17.6	[366]
0.2	0.5	2.87×10^2	3.25×10^2	373–1173	18.7	[366]
0.2	0.6	4.14×10^2	4.55×10^2	373–1173	20.0	[366]
0.2	0.7	7.43×10^2	7.76×10^2	373–1173	20.3	[366]
0.2	0.8	1.05×10^3	9.95×10^2	373–1173	20.7	[366]
				470–1070	15.4	[90]
0.2	0.9	1.14×10^3	1.07×10^3	373–1173	20.1	[366]
0.2	1.0	1.37×10^3	1.24×10^3	373–1173	19.7	[366]
		1.69×10^3	1.52×10^3	303–1273	18.5	[136]
0.3	0.2	2.40×10^2	2.05×10^2	373–973	14.6	[365]
		1.59×10^2	1.59×10^2	303–1273	16.0	[136]
0.3	1.0	1.97×10^3	1.68×10^3	303–1273	19.2	[136]
				303–1073	17.5	[306]
				303–1273	19.2	[306]
0.4	0.2	3.35×10^2	2.79×10^2	373–873	15.3	[365]
		2.75×10^2	3.33×10^2	303–1273	17.5	[136]
		4.60×10^2	3.30×10^2	973	15.3	[109]
				1273	19.9	[109]
0.4	1.0	2.03×10^3	1.60×10^3	303–1273	20.5	[136]
0.5	1.0	1.90×10^3	1.36×10^3	303–1273	22.3	[136]
0.6	0.2			373–673	16.8	[365]
0.6	0.8			373–1273	21.2	[113]
0.6	1.0	1.81×10^3	1.16×10^3	303–1273	25.1	[136]
0.7	0	61	44	303–1273	25.6	[136]
0.7	0.1	90	61	303–1273	24.8	[136]
0.7	0.2	51	46	303–1273	27.1	[136]
0.7	0.3	63	54	303–1273	27.1	[136]
0.7	0.4	95	83	303–1273	23.9	[136]
0.7	0.5	1.32×10^2	93	303–1273	23.5	[136]
0.7	0.6	1.73×10^2	1.29×10^2	303–1273	24.1	[136]
0.7	0.7	2.86×10^2	2.17×10^2	303–1273	24.7	[136]
0.7	0.8	4.80×10^2	3.88×10^2	303–1273	21.0	[136]
0.7	0.9	1.37×10^3	8.37×10^2	303–1273	19.2	[136]
0.7	1.0	1.47×10^3	9.12×10^2	303–1273		[136]
				303–1273	25.0	[367]
0.8	1.0	8.10×10^2	5.78×10^2	303–1273	25.6	[136]
0.9	1.0	3.35×10^2	1.91×10^2	303–1273	26.0	[136]

from $A(Co,Fe)O_{3-\delta}$ (A = Sr, Ba). The roles of A^{2+} cation size and its matching to Ln^{3+} radius are still disputed. In addition to experimental limitations associated with the partial conductivity measurements when the ion transference numbers are as low as 10^{-7}–10^{-5}, the disagreements in literature data may partly result from local vacancy ordering in the oxygen sublattice, cation demixing under non-equilibrium conditions, and phase separation in the intermediate-

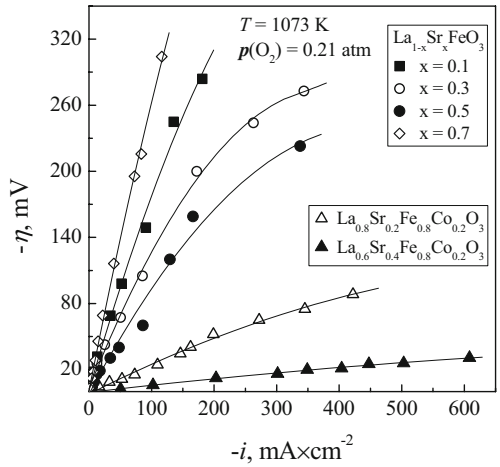

Fig. 6 Current dependence of the cathodic overpotentials of porous $La_{1-x}Sr_xFeO_{3-\delta}$ [51] and $La_{1-x}Sr_xFe_{0.8}Co_{0.2}O_{3-\delta}$ [90, 111] electrodes in contact with YSZ and doped ceria electrolytes, respectively

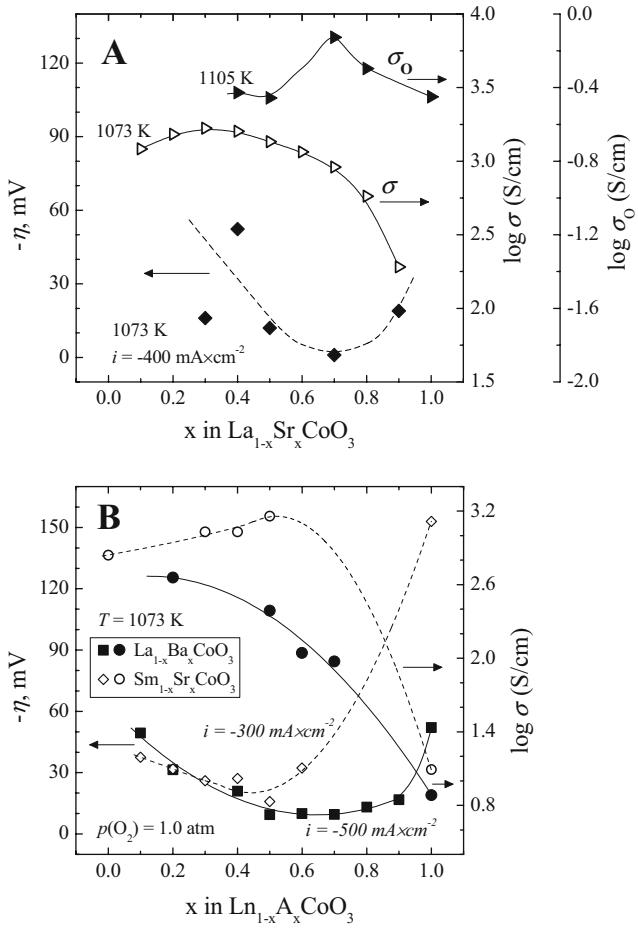

Fig. 7 Dopant concentration dependencies of the cathodic overpotentials of $La_{1-x}Sr_xCoO_3$|YSZ half cells [51, 122], and total and partial oxygen ionic conductivities of $La_{1-x}Sr_xCoO_3$ ceramics [136, 137] at atmospheric oxygen pressure (**a**), and typical relationships between polarization of porous cobaltite cathodes in contact with LSGM-based electrolytes and total conductivity of $Sm_{1-x}Sr_xCoO_3$ [120] and $La_{1-x}Ba_xCoO_3$ [138] (**b**)

temperature range [21, 143–146]. Analogously to ferrite-based systems, the latter phenomena are all affected by the cobaltites thermodynamic properties correlating with the tolerance factors and A-site cation radii, but also by the materials microstructure. As a consequence, while the positive impact of Ba^{2+} doping on the oxygen reduction kinetics was established by numerous researchers [131, 138, 147, 148], data on the ionic transport in $(Ba,Sr)(Co,Fe)O_{3-\delta}$ perovskites are quite contradictory (e.g., [149–152]). On the other hand, extensive Ba^{2+} substitution for Sr^{2+} in the IT SOFC electrode materials is very unlikely due to fast interaction with CO_2 and water vapor present in air [153].

The interaction mechanisms between the cobaltite-based cathodes and solid electrolytes are, in general, similar to those in Fe- and Mn-containing electrodes, whereas the cation interdiffusion and topotactic reaction rates are often enhanced owing to lower thermodynamic stability of the cobaltite phases [25, 55, 98, 106, 113, 122, 154–159]. In particular, the cobaltite electrodes may easily react with zirconia compared to LSM; no blocking layers are formed in the electrochemical cells with CeO_2- or $LaGaO_3$-based solid electrolytes, but progressive Co diffusion may have a deteriorating influence on the SOFC performance. These effects make it necessary to decrease the cell fabrication temperature and to use sintering aids, as for the majority of other oxide electrode materials.

Typical examples illustrating the superior performance of porous cobaltite cathodes in contact with various solid electrolytes are presented in Figs. 7 and 8a and in Table 3. The high electrochemical activity may be of great interest for practical applications, provided that matching of thermal expansion can be achieved via the development of electrolyte-containing composites. The latter approach is, indeed, used successfully for the model cells (e.g., [160, 161]), although moderate solid electrolyte additions comparable to the percolation threshold are hardly expected to decrease the average TECs down to any acceptable level. Another necessary comment relates to the absence of direct correlations between the bulk transport properties and electrocatalytic behavior of cobalt-containing electrodes, which are often visible if comparing different groups of the electrode materials [25, 90, 162]. For instance, the maximum power density in LSGM-based SOFCs with $(La,Sr)MO_{3-\delta}$ cathodes at 1273 K increased in the sequence M = Cr < Mn < Fe < Co [120, 163]; similar trends are known for the electronic conductivity, oxygen ion diffusivity, and anion deficiency [25, 164, 165]. On the contrary, lowest polarization resistance in $(Ln,Sr)CoO_3$-based series was repeatedly found for the compositions where Ln^{3+} cation radius is smaller than that of La^{3+}, including Sm, Nd, or Pr [147, 148, 162, 163, 166, 167]. For $Y_{0.8}Ca_{0.2}Co_{1-x}Fe_xO_{3-\delta}$ perovskites stable in

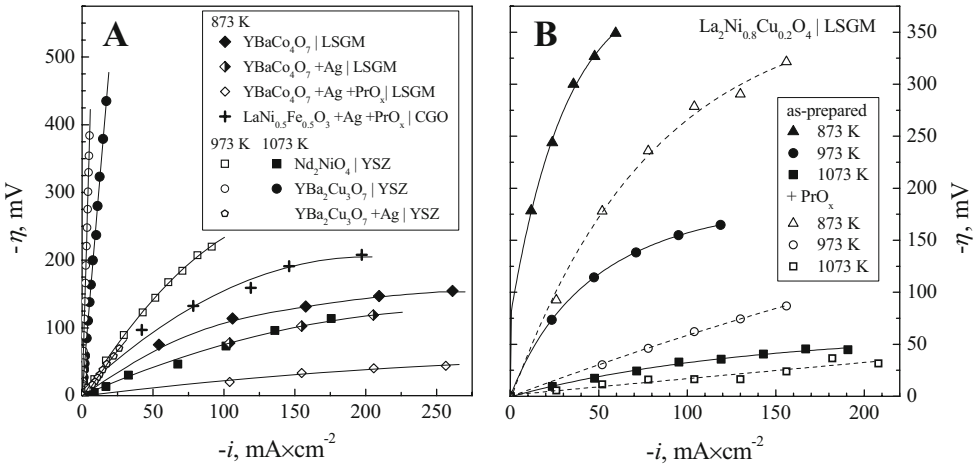

Fig. 8 **a**, **b** Comparison of the cathodic overpotentials for selected Co-, Ni-, and Cu-containing electrodes after fabrication and after modification with metallic silver and praseodymia, at atmospheric oxygen pressure [90, 131, 194, 196, 214]

air at x=0.1–0.7, the electrochemical activity is low, comparable to manganite electrodes [118]; a poor performance was also reported for $Y_{0.9}Co_{0.5}Mn_{0.5}O_{3-\delta}$ [123]. The observed tendencies show that, in addition to the species occupying cobalt and oxygen sublattices, the cathodic kinetics is significantly influenced by specific electrocatalytic properties of lanthanide cations or surface clusters comprising Ln^{3+}. These conclusions are in agreement with numerous experimental and theoretical results demonstrating that the performance of cobaltite and ferrite electrodes is essentially governed by the exchange processes at the electrode and electrolyte surfaces and by ion transfer across the cathode/electrolyte interface [21, 26, 111, 124, 131, 147, 162, 168–171]; the role of bulk ionic transport in the electrode material crystal lattice seems important, but less critical with respect to these steps. Due to the very high electronic conductivity, the hole transport may not be rate limiting and exhibit no correlations with the electrochemical behavior (Fig. 7).

Nickelates and cuprates

The thermodynamic stability of transition metal-containing perovskites, $LnMO_3$, and the average oxidation state of M-site cations under cathodic conditions increases as Cu < Ni < Co < Fe < Mn [21, 23, 25, 39, 115, 172, 173]. At oxygen pressures close to atmospheric, $LaNiO_{3-\delta}$ is only stable below 1130–1250 K; heating leads to its decomposition into K_2NiF_4-type $La_2NiO_{4+\delta}$ and NiO via the separation of $La_4Ni_3O_{10-\delta}$ and $La_3Ni_2O_{7-\delta}$ phases at intermediate stages [23, 25, 174–176]. As for $LaNiO_{3-\delta}$, the latter Ruddlesden–Popper compounds display attractive electrochemical and transport properties, but suffer from insufficient phase stability in the range of temperatures and oxygen chemical potentials necessary for the SOFC applications [23, 25, 175–180]. Decreasing the Ln^{3+} cation radius and acceptor-type doping both cause further decreases in the thermodynamic stability. The decomposition limits can be shifted towards

Table 3 Examples of the maximum power density in H_2-fueled SOFCs with cobaltite cathodes

Cathode	Solid electrolyte/ thickness (mm)	Anode	T, K	Maximum power density, W/cm^2	Ref.
$La_{0.9}Sr_{0.1}CoO_3$	YSZ/0.5	Ni	1273	0.39	[163]
			1073	0.05	
$La_{0.9}Sr_{0.1}CoO_3$	LSGM/0.5	Ni	1273	0.93	[163]
			1073	0.38	[120]
$La_{0.6}Sr_{0.4}CoO_3$	LSGM/0.5	Ni	1273	0.71	[163]
			1073	0.21	
$La_{0.6}Sr_{0.4}CoO_3$	LSGM/0.5	Co	1273	0.53	[163]
$La_{0.2}Sr_{0.8}CoO_3$	LSGM/0.5	Ni	1073	0.44	[138]
$La_{0.2}Ca_{0.8}CoO_3$	LSGM/0.5	Ni	1073	0.46	[138]
$La_{0.4}Ba_{0.6}CoO_3$	LSGMC[a]/0.4	Ni	873	0.12	[138]
$La_{0.2}Ba_{0.8}CoO_3$	LSGM/0.5	Ni	1073	0.52	[138]
$Sm_{0.6}Sr_{0.4}CoO_3$	LSGM/0.5	Ni	1073	0.44	[163]
$Sm_{0.5}Sr_{0.5}CoO_3$	LSGM/0.5	Ni	1073	0.53	[147]
			873	0.08	[120]
$Sm_{0.5}Sr_{0.5}CoO_3$	CGO/0.03	Ni–CGO	873	0.27	[121]

[a] $La_{0.8}Sr_{0.2}Ga_{0.8}Mg_{0.115}Co_{0.05}O_3$

higher temperatures and lower $p(O_2)$ by extensive substitution in the Ni sublattice. In particular, $La(Ni,M)O_{3-\delta}$ (M = Ti–Co, Ga) containing 50–60% Ni cations retain perovskite structure at elevated temperatures [25, 115, 174, 181–187], while the ionic and electronic conductivities tend to decrease on doping. Consequently, despite potential thermomechanical problems during sintering as mentioned above, perovskite-type $LaNi_{1-x}Fe_xO_{3-\delta}$ (x=0.5–0.6) are considered as an interesting group of the IT SOFC cathode materials [85, 90–92, 174, 182].

In ternary Ln–M–O (Ln = La, Pr, Nd; M = Ni, Cu) systems, the K_2NiF_4-type compounds are most stable in oxidizing and moderately reducing atmospheres [23, 25, 175, 176]. The solid solution formation domains in $La_{2-x}A_xNi_{1-y}M_yO_{4\pm\delta}$ series at atmospheric oxygen pressure correspond to x=0–1.4 for A = Sr; $x\leq1.0$ for A = Ba; $x\leq0.5$ for A = Ca; $y\leq0.1$ and 0.2 for M = Fe and Co at x=0, respectively; and y=0–1.0 for M = Cu at x=0 [23, 25, 39, 188–190]. The total conductivity of K_2NiF_4-type nickelates remains predominantly p-type electronic in the entire $p(O_2)$ range where these phases exist; the hole transport is lower than that in the perovskite analogues, but still sufficient for practical applications. Moderate A^{2+} doping leads to a higher conductivity and lower oxygen content, with a negative impact on the oxygen diffusivity which is substantially determined by the interstitial anion migration [189, 191–193]. On the other hand, although the substitution of nickel with higher-valence cations rises interstitials concentration, an increase in the ionic transport is only observed at temperatures above 1100 K [192, 193]. The maximum ionic conduction in Ln_2NiO_4-based systems is thus characteristic of the compositions with modest dopant content, particularly for the parent nickelate phases. The corresponding σ_o values are 4–10 times lower if compared to highly oxygen-deficient $SrCo(Fe)O_{3-\delta}$ and $Sr(La)CoO_{3-\delta}$ perovskites, but are quite similar to those in $(La,Sr)FeO_{3-\delta}$ [80, 188, 191–195]. In combination with relatively low TECs (Table 4), this feature may provide serious advantages. One should also mention that doping with copper considerably improves sinterability [188, 196], enabling to reduce the electrode fabrication temperature and to minimize interaction with solid electrolytes.

Figures 8 and 9 present selected data on the electrochemical behavior of several nickelate-based electrodes. A relatively low polarization resistance at 773–1073 K was observed for porous $Ln_2NiO_{4+\delta}$ (Ln = La, Nd, Pr) layers deposited onto YSZ, with a minimum for praseodymium nickelate [194]. Note that high performance of the latter composition may be significantly contributed by the metastability of $Pr_2NiO_{4+\delta}$, which decomposes at temperatures below 1150–1200 K into electrocatalytically active PrO_x and $Pr_4Ni_3O_{10-\delta}$ having higher ionic and electronic conductivities [180]. For instance, the electrochemical activity of $LaNi_{0.5}Fe_{0.5}O_{3-\delta}$ [90] and $La_2Ni_{0.8}Cu_{0.2}O_{4+\delta}$ [196] cathodes can be enhanced by surface modification with praseodymium oxide, confirming the role of oxygen surface exchange as a rate-determining factor [196, 197]. Ageing tests of $Ln_2NiO_{4+\delta}$ electrodes under DC conditions showed a

Table 4 Average TECs of selected Ni- and Cu-containing materials in air

Composition	T, K	$\overline{\alpha}\times10^6$, K^{-1}	Ref.
La_2NiO_4	290–1170	13.7	[191]
La_2NiO_4	300–1270	13.0	[188]
La_2NiO_4	370–720	13.7	[195]
	920–1220	14.4	
$La_{1.7}Sr_{0.3}NiO_4$	300–1270	11.3	[39]
$La_{1.6}Sr_{0.4}NiO_4$	300–1270	13.2	[39]
$La_{1.4}Sr_{0.6}NiO_4$	300–1270	11.0	[39]
$La_2Ni_{0.98}Fe_{0.02}O_4$	300–1100	13.2	[192]
$La_2Ni_{0.90}Fe_{0.10}O_4$	370–1120	13.8	[195]
$LaPrNi_{0.90}Fe_{0.10}O_4$	300–1100	13.4	[192]
$La_{1.9}Sr_{0.1}Ni_{0.90}Fe_{0.10}O_4$	300–1100	12.7	[192]
$La_2Ni_{0.50}Cu_{0.50}O_4$	290–1270	12.8	[188]
La_2CuO_4	290–520	8.6	[188]
	520–1170	13.8	
Pr_2CuO_4	300–1070	10.2	[192]
Nd_2CuO_4	300–1050	10.1	[192]
$La_2Cu_{0.98}Co_{0.02}O_4$	300–460	7.1	[192]
	470–1050	12.2	
$La_2Cu_{0.90}Co_{0.10}O_4$	300–1080	13.2	[192]
$LaNi_{0.7}Fe_{0.3}O_3$	300–1270	12.1	[173]
$LaNi_{0.5}Fe_{0.5}O_3$	300–1270	10.9	[173]
$LaNi_{0.5}Fe_{0.5}O_3$	300–1100	11.9	[90]
$LaNi_{0.6}Co_{0.4}O_3$	300–1270	15.0	[173]
$LaNi_{0.6}Mn_{0.4}O_3$	300–1270	10.8	[173]
$La_{0.6}Sr_{0.4}Ni_{0.5}Mn_{0.5}O_3$	300–1100	12.1	[181]
$La_{0.6}Sr_{0.4}Ni_{0.3}Mn_{0.7}O_3$	350–1100	12.5	[181]

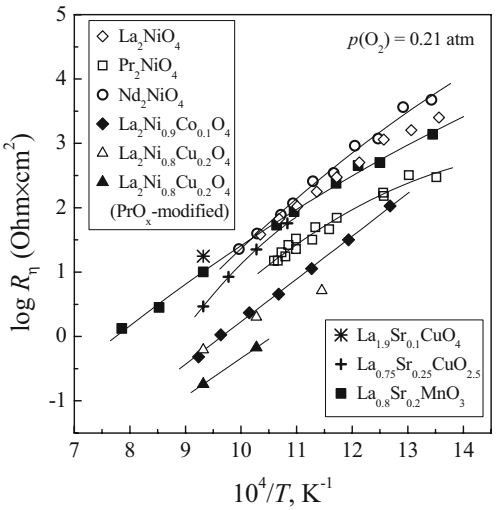

Fig. 9 Temperature dependencies of the area-specific polarization resistance of porous oxide cathodes in air [42, 194, 196, 198, 215, 370]. All data correspond to the electrochemical cells with YSZ solid electrolyte, except for $La_2Ni_{0.9}Co_{0.1}O_{4+\delta}$ and $La_2Ni_{0.8}Cu_{0.2}O_{4+\delta}$ measured in contact with LSGM

decrease in the polarization resistance without any visible interaction with zirconia [194]. However, the electrode–electrolyte interaction may still have a crucial importance. As an example, the area-specific resistivity of porous $La_2Ni_{0.9}Co_{0.1}O_{4+\delta}$ was found lower in contact with $La_{0.9}Sr_{0.1}Ga_{0.8}Mg_{0.2}O_{3-\delta}$ electrolyte compared to $Ce_{0.9}Gd_{0.1}O_{2-\delta}$ at 773–1073 K [198]; long-term annealing of both cells at 1273 K results in the separation of secondary phases, $La_3Ni_2O_7$ and La_2O_3, due to nickel diffusion into the electrolyte ceramics. Opposite results were reported for $(Ln,Nd)_2NiO_{4+\delta}$ in contact with LSGM, where the poor electrochemical performance in comparison with samaria-doped ceria was attributed to the materials reactivity [199]. Whatever the phase interaction kinetics, the incorporation of doped ceria components into nickelate electrodes and the formation of ceria interlayers decrease cathodic polarization, as for many other oxide electrodes in the intermediate-temperature range [199, 200].

The ternary and quaternary Cu-containing oxide systems display several distinctive features relevant for the SOFC developments (e.g., [23, 25, 201–205] and references therein). First, relatively low melting points characteristic of all these systems may limit the cell fabrication and operation temperatures and lead to a fast electrode sintering and microstructural degradation at 1050–1200 K. This makes it possible to use minor additions of Cu-containing sintering aids or cathode materials where Cu^{2+} cations are incorporated in the lattice [25, 30, 50, 159, 180, 188, 196], but may hamper application of cuprate-based electrodes. Second, no perovskite-type compounds exist in the Ln–A–Cu–O systems at oxygen pressures close to atmospheric and SOFC operation temperatures; the solubility of Cu^{2+} in most perovskite phases is usually low, ≤30%. In spite of complex phase relationships and rich crystal chemistry in the cuprate materials, the number of high-conductivity compositions stable under the IT SOFC cathodic conditions is not very large, including primarily K_2NiF_4-type $(Ln,A)_2CuO_{4\pm\delta}$ (Ln = La–Sm; Ln = Sr, Ba) and various derivatives of layered $LnA_2Cu_3O_{7-\delta}$ formed in the systems with Y^{3+} and smallest lanthanide cations. As for perovskites, the thermodynamic and thermal stability of $Ln_2CuO_{4+\delta}$ decreases with decreasing Ln^{3+} radius; the dopant solubility in both sublattices is quite similar to that of $Ln_2NiO_{4+\delta}$ [23, 201–203, 206–208]. The total conductivity of $La_2CuO_{4+\delta}$, which exhibits a small oxygen excess in air, has pseudometallic character (Fig. 1) and is considerably lower than that of lanthanum nickelate [23, 25, 188]. Again, moderate acceptor-type doping enhances the *p*-type electronic transport, whereas decreasing Ln^{3+} size has an opposite effect. The oxygen diffusion and surface exchange in all cuprates are rather slow and tend to decrease when the Ln^{3+} radius decreases [188, 192, 208–213]. In the case of $La_{2-x}Sr_xCuO_{4\pm\delta}$, the ion diffusivity becomes slightly higher on modest Sr doping ($x<0.1$) and drops with further additions; the substitution of copper with higher-valence cations has often positive impact on the ionic transport, thus indicating relevance of both vacancy and interstitial migration mechanisms. Note that increasing oxygen content in another well-known cuprate, $YBa_2Cu_3O_{7-\delta}$, also results in higher oxygen permeability and ionic conductivity [212].

Most layered cuprates are thermomechanically compatible with solid oxide electrolyte ceramics (Table 4). Nonetheless, the performance of cuprate cathodes is usually worse compared to their nickelate analogues (e.g., [214, 215]). This is associated, first of all, with lower ionic and electronic transport and with poorer stability. The latter factor promotes interaction with solid electrolytes, especially when a liquid phase is formed during fabrication; in addition, an accelerated degradation due to progressive sintering under operating conditions may take place. The potential applications include, hence, IT SOFC where the maximum operation temperature is limited to 950–1050 K, provided a deep optimization of the cell processing conditions. For example, thick diffusion layers consisting of $SrZrO_3$ and $La_2Zr_2O_7$ were found to form at the interface between $La_{1.9}Sr_{0.1}CuO_4$ and YSZ after firing at 1373 K, deteriorating electrochemical properties [215]. On the contrary, a low polarization resistance, 0.16 Ω cm^2 at 973 K and 1.2 Ω cm^2 at 773 K in air, was reported for $La_{1.7}Sr_{0.3}CuO_{4-\delta}$ cathodes sintered onto CGO at 1170 K [216].

Composite cathodes: selected aspects

The key directions in the IT SOFC developments relate to multiphase composite electrodes comprising, at least, one electronically conducting material and a solid electrolyte component. The advantages of this approach were demonstrated for all types of the parent cathode compositions [61–66, 200, 217–223]. The introduction of the solid electrolyte component provides a substantial enlargement of the electrochemical reaction zone, enhances the electrode microstructural stability and adherence to the electrolyte, enables to adjust TECs, and mitigates strains caused by the electrode chemical expansion induced by overpotential variations. Further improvements can be achieved via the incorporation of nanocrystalline catalyst particles onto the electrode and electrolyte surfaces and into pores, by the creation of compositional, particle size and porosity gradients, and using various chemical treatments modifying the surface composition and increasing connectivity of the constituent particles. One should mention, however, that an extensive use of nanoscale engineering methods may lead to instabilities even in the intermediate-temperature range (e.g., [221–223] and references cited), thus making it necessary to include long-term testing in the standard procedures for IT SOFC electrode characterization.

Figure 10 illustrates typical trends observed for the dual-phase composite cathodes. The general tendencies are in agreement with theoretical calculations using a random

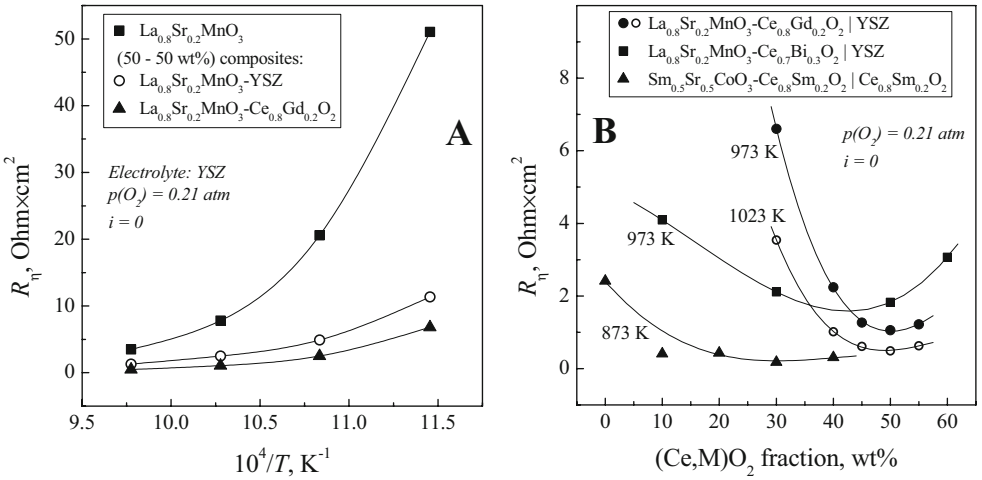

Fig. 10 Examples of the polarization resistance vs. temperature (**a**) and composition (**b**) for various composite cathodes containing YSZ and $Ce(M)O_{2-\delta}$ (M = Sm, Gd, Bi) ionic conductors [217–219]

resistor networks model [224], predicting minimum R_η for 30–60 vol.% fraction of the electronically conducting phase; further IC additions result in a drastic rise of the ohmic resistance and in the electronic transport limitations to electrochemical kinetics. However, there exist additional factors affecting the composite performance, primarily the components interaction, grain-boundary resistivity phenomena, and possible alterations in the reaction mechanisms (e.g., [225–229]); precise separation of the corresponding contributions to the overall electrode resistance is usually impossible. For instance, the better performance of ceria-containing composites in comparison with LSM–YSZ (Fig. 10) results from both an absence of ion-blocking layers and the higher ionic conductivity of doped ceria.

Finally, while the formation of composite cathodes is the only viable way to use cobaltite- and ferrite-based materials having excessively high TECs (Table 2), such composites provide superior electrochemical activity as the role of catalytically active electronic conductor remains important due to critical effects of the reaction zone width in the vicinity of triple-phase boundaries (TPBs) and to correlations between oxygen exchange and ion diffusion. As an example, the polarization resistance of $La_{0.6}Sr_{0.4}Co_{0.2}Fe_{0.8}O_{3-\delta} - Ce_{0.8}Gd_{0.2}O_{2-\delta}$ (50–50 vol.%) was reported as low as 0.33 and 0.01 Ω cm^2 at 873 and 1023 K, respectively [230]. The $La_{0.6}Sr_{0.4}Co_{0.8}Fe_{0.2}O_{3-\delta} - Ce_{0.8}Gd_{0.2}O_{2-\delta}$ (70–30 wt.%) composite applied onto $Ce_{0.8}Sm_{0.2}O_{2-\delta}$ with subsequent deposition of metallic Ag, showed R_η lower than 1 Ω cm^2 at 873 K [231]; the polarization resistance of $Sm_{0.5}Sr_{0.5}CoO_{3-\delta} - Ce_{0.9}Sm_{0.1}O_{2-\delta}|Ce_{0.9}Gd_{0.1}O_{2-\delta}$ half cells was approximately 0.4 Ω cm^2 at 973 K [232]. Even moderate (10 wt.%) $Ce_{0.8}Sm_{0.2}O_{2-\delta}$ additions into $Sm_{0.5}Sr_{0.5}CoO_{3-\delta}$ cathode deposited onto $Ce_{0.8}Sm_{0.2}O_{2-\delta}$ electrolyte had a dramatic effect on the polarization; the minimum R_η value, <0.18 Ω cm^2 at 873 K, was found for 30 wt.% $Ce_{0.8}Sm_{0.2}O_{2-\delta}$ [219].

Anodes

Conventional cermets

The ceramic–metal composites (cermets) containing YSZ and Ni, where the metallic phase acts as electronic conductor and catalyst, are the common SOFC anode materials up to now [1–5, 19–21, 233–236]. As for the oxide composite electrodes, zirconia additives have a number of important functions listed above and are necessary to achieve sufficient power density and durability, particularly to adjust thermal expansion (Table 5). Again, since the composite layers should provide percolation paths for electrons, oxygen ions, and gas, the cermet performance is strongly dependent on the microstructure-related factors, including processing conditions and pre-history; this leads often to discrepancies in the

Table 5 Average thermal expansion coefficients of selected SOFC anode materials and their components

Composition	T, K	$\overline{\alpha} \times 10^6$, K^{-1}	Ref.
Ni	–	16.5	[248]
$Zr_{0.85}Y_{0.15}O_2$	303–1273	10.9	[306]
$Zr_{0.85}Y_{0.15}O_2$	323–1273	10.3	[368]
Ni–$Zr_{0.85}Y_{0.15}O_2$ (40–60 vol.%)	303–1273	12.6	[306]
$Zr_{0.94}Y_{0.06}O_2$	298–1273	10.5	[248]
Ni–$Zr_{0.94}Y_{0.06}O_2$ (30–70 vol.%)	298–1273	12.7	[248]
Ni–$Zr_{0.94}Y_{0.06}O_2$ (40–60 vol.%)	298–1273	13.1	[248]
Ni–$Zr_{0.94}Y_{0.06}O_2$ (45–55 vol.%)	298–1273	13.3	[248]
$La_{0.9}Sr_{0.1}CrO_3$	303–1273	10.7	[306]
$La_{0.79}Sr_{0.20}CrO_3$	623–1273	11.1	[306]
$La_{0.7}Ca_{0.3}Cr_{0.5}Ti_{0.5}O_3$	303–1273	10.1	[306]
$La_{0.7}Sr_{0.3}Cr_{0.8}Ti_{0.2}O_3$	303–1273	10.7	[306]
$(La_{0.75}Sr_{0.25})_{0.95}Cr_{0.5}Mn_{0.5}O_{3-\delta}$	373–923	10.8	[310]
	923–1223	12.7	
	1223–1523	14.1	

literature data. One standard approach to minimize the interfacial resistance of Ni–YSZ anodes relates to increasing TPB length [237]. This can be achieved, in particular, using small Ni particles and high YSZ to Ni particle ratio (Fig. 11). For example, a mixture of fine and coarse YSZ particles was suggested [238] to tune the microstructure and properties of the cermets. On the other hand, a significant improvement was observed when fabricating the anodes from mechanically processed powder, with a resultant microstructure comprising submicron Ni and YSZ particles and uniformly distributed micron-sized pores [239]. A variety of graded functional layers enhancing the SOFC performance are also known, although the approaches to their architectural and morphological optimization are different and, often, contradictory (e.g., [240–242] and references cited). Hence, attention is centered on theoretical modeling of the porous cermets in order to formulate guidelines for the anode design. The simulation methods can be classified according to the type of system representation [243]; particular cases include the use of macroscopic averaged descriptions of disordered electrode structure, modeling of the anode material corrugated layers covered by a thin electrolyte film or vice versa (thin film models), and simulating random packing of particles (Monte Carlo calculations). One important conclusion was drawn from the impedance network modeling [244], which showed that the electrode response may be more complex than that for a single interface; distortions of the impedance spectra and/or extra arcs appear when the system is close to or below the percolation threshold for electronic conduction. Ascribing the electrode signal elements visible in the Nyquist plots to any definite steps of the electrochemical process [245] may thus be questionable. For the cermets where components

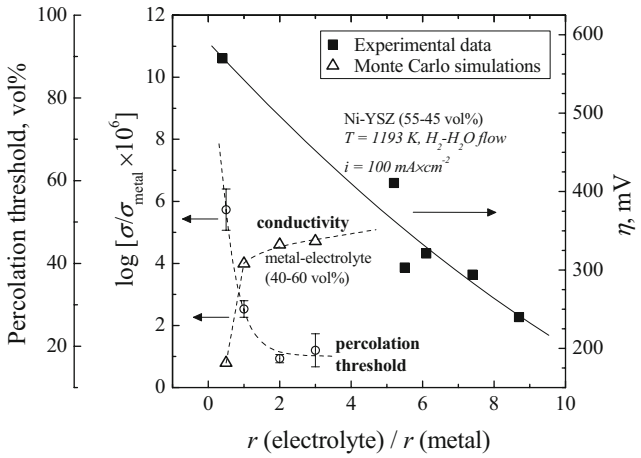

Fig. 11 Relationships between the relative electrical conductivity of metal–electrolyte (40–60 vol.%) composite and metal percolation threshold estimated by the Monte Carlo simulations for random packing [249], and experimentally measured overpotentials of Ni–$Zr_{0.85}Y_{0.15}O_2$ anodes [237], as functions of the particle size ratio

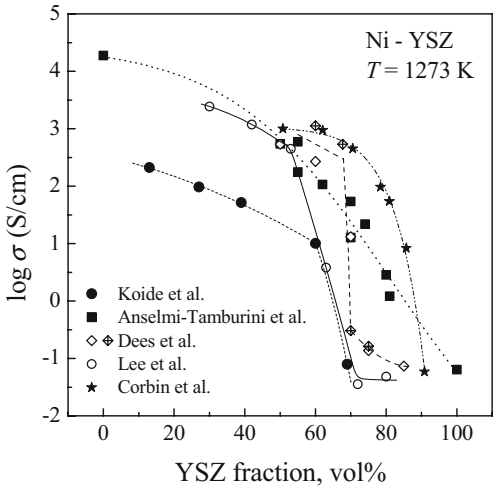

Fig. 12 Total conductivity of Ni–YSZ cermets with various microstructures vs. YSZ content in H_2–H_2O and N_2 atmospheres [238, 249–251, 368]

have similar grain sizes, the percolation threshold is expected to correspond to approximately 30 vol.% metallic phase [246]. This estimation agrees with experiments (Fig. 12), but a substantial scatter is always observed due to microstructural differences. The electrical conductivity of porous Ni–YSZ composites in hydrogen was reported to exhibit a semiconductor-like behavior up to 30 vol.% Ni and to become metallic when Ni fraction increases to 50% [247], while other authors [248, 249] observed metallic behavior even for the compositions containing 20–30 vol.% Ni. The use of combustion synthesis [249] and Ni-coated graphite particulates [250] enabled to alter the electrical properties in the vicinity of nickel percolation limit, increasing the conductivity of zirconia-rich materials. The YSZ fraction optimum for electrochemical performance is also dependent on the anode processing conditions and varies usually in the range of 30–60 vol.% (Fig. 13). For instance, minimum

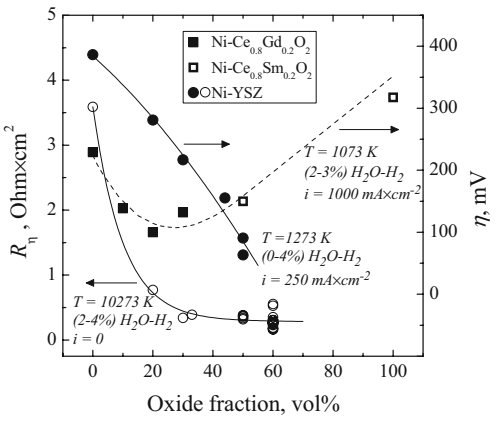

Fig. 13 Polarization resistance and overpotentials of Ni–YSZ|YSZ [19, 271, 354, 371–373], Ni–CGO|LSGM [284], Ni–$(Ce,Sm)O_{2-\delta}$|LSGM [374] and $(Ce,Sm)O_{2-\delta}$|YSZ anodes [255]

polarization resistance at 1273 K was found for 60 vol.% YSZ, whereas the ohmic resistivity decreased with Ni additions as expected [251].

At elevated temperatures, the microstructure and properties of Ni–YSZ cermets with high nickel content undergo fast degradation due to coarsening of the metal particles. Another factor making it necessary to decrease metal concentration in the cermets is the stability to redox cycling which may cause microstructural reconstruction, strains and failure, accompanied with rising overpotentials. As an example, 33% decrease in the conductivity measured at 298 K was revealed for reduced 56 wt.% NiO–YSZ after an exposure at 1273 K in 3% H_2–H_2O–Ar for 4,000 h [252]. The rate of increasing overpotential of $Ni-Zr_{0.85}Y_{0.15}O_{2-\delta}$ (51–49 vol.% or 67 wt.% NiO) in 50%H_2–N_2 atmosphere at 1200–1280 K and 300 mA/cm^2 was as high as 14 μV/h [253]; the polarization of Ni–YSZ (65–35 mol%) anode at 1223 K increased by 18% after triple redox cycling [254]. Such problems are typical, to a different extent, for all cermet electrodes; although the redox stability of noble metal-containing composites is much better, these are excluded from consideration in this review as their wide application is unlikely due to economic reasons. Taking into account the durability issues related to carbon deposition and sulfur poisoning, continuous efforts are being made since the 1970s to develop optimized anode formulations, particularly via the use of other transition-metal components [1, 6, 19, 27, 30, 255–263]. The copper-based anodes, which may be of interest for hydrocarbon-fueled SOFCs in combination with ceria catalysts due to low Cu activity towards C–C bond formation, exhibit however poor electrochemical properties; the introduction of Fe and Co also leads to serious drawbacks associated primarily with the metal oxidation under high current densities. In terms of phase interaction with the fluorite-type solid electrolytes, most transition metal-based cermets exhibit quite similar behavior, at least at temperatures above 1000 K (e.g., [30, 158] and references cited). A considerably higher reactivity with cermets is known for the gallate electrolytes where the reaction layers do not display a critical increase of the *n*-type electronic conductivity in reducing conditions, but may partly block ion transfer and should be avoided via the deposition of buffer sub-layers, such as doped ceria [104, 186, 264–268]. The relatively poor electrochemical performance of Ni-containing cermets in contact with apatite-type silicate electrolytes [269] may also originate from the materials interaction, including silica diffusion [270], though information on the relevant mechanisms is still very scarce. Another approach for the cermet optimization is to increase *n*-type electronic conduction in the ZrO_2-based components by doping and, thus, to expand the anodic reaction zone [263, 271–274]. However, the incorporation of cations forming redox couples under anodic conditions, such as $Ce^{3+/4+}$, $Ti^{3+/4+}$, or $Nb^{4+/5+}$, leads to decreasing ionic conduction in the cubic zirconia [30]; the cumulative effects of such modifications on the anode polarization are rather negligible. Nevertheless, Ti doping makes it possible to improve mechanical stability of the cermets [263, 271].

Ceria-based anode materials

Since the first attempts to use ceria for the SOFC anodes in the 1960s [18, 19, 30, 275], introducing $CeO_{2-\delta}$-based additives and layers is widely considered among the most promising directions in the anode developments [6, 9, 11, 17, 235, 259, 265, 276–282]. The advantages are associated, first of all, with a very high catalytic activity of ceria to the combustion reactions involving oxygen, particularly to carbon oxidation beneficial for the fuel cells operating on hydrocarbons and biogas. In addition, reduced $CeO_{2-\delta}$ and its derivatives possess a substantial mixed oxygen ionic and *n*-type electronic conductivity; the transport properties and reducibility can be enhanced by acceptor-type doping [17, 158], which clearly has a positive impact on the electrode performance (Fig. 14). For example, maximum power density for $Ce_{1-x}Sm_xO_{2-\delta}$ (x=0–0.4) anodes in contact with YSZ electrolyte at 1073–1273 K in humidified H_2 was found for the composition with x=0.2 [283]. On the other hand, although no carbon deposition was detected on $Ce_{0.6}Gd_{0.4}O_{2-\delta}$ electrode after testing for 1,000 h at 1273 K and steam to carbon ratio of 0.3, the electrocatalytic activity of gadolinia-doped ceria without extra additives was revealed insufficient to provide direct CH_4 oxidation [277]. Note that the electronic conduction in ceria solid solutions is also lower than necessary to avoid critical ohmic losses and/or current constriction effects on the overall anodic polarization, thus requiring to

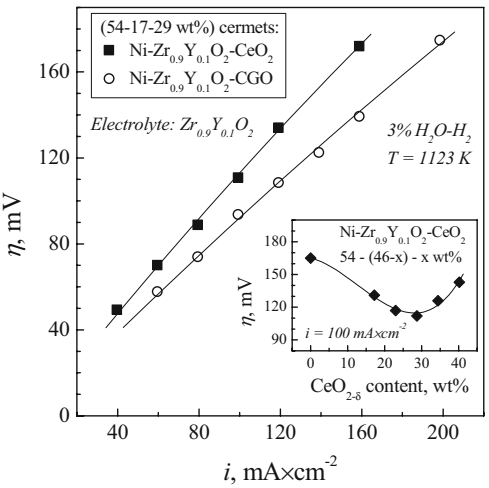

Fig. 14 Anodic overpotential vs. current density dependencies for two cermet compositions, containing 29 wt.% of $CeO_{2-\delta}$ or $Ce_{0.8}Gd_{0.2}O_{2-\delta}$ (CGO), in contact with YSZ electrolyte at 1123 K [285]. *Inset* shows anodic overpotentials of Ni–YSZ–$CeO_{2-\delta}$ cermet layers at 100 mA/cm^2

introduce an additional metal component. Figure 15 presents selected data on the performance of YSZ- and (Ce,Sm)O_2-based anodes.

Comparative tests of the electrode layers containing nickel and various mixed-conducting components showed that the cermets with $Nd(Ca)Ga(Co,Mg)O_{3-\delta}$ perovskites or $Gd_2Ti_2O_{7-\delta}$ pyrochlore perform substantially worse than those with ceria [284]; the overpotentials of 95 wt.% Ni–5 wt.% $Ce_{0.8}Ln_{0.2}O_{2-\delta}$ (Ln = Sm, Gd) anodes in contact with LSGM were slightly lower for Ln = Sm. Qualitatively similar conclusions on the role of ceria-based additives were drawn [259, 285] studying three-phase cermets with Ni, Cu, YSZ, CGO, and other mixed conductors, including fluorite-related $TbZrO_{4-\delta}$ [286], zircon-type $Ce_{0.8}Ca_{0.2}VO_{4+\delta}$ [287], $Gd_{1.86}Ca_{0.14}Ti_2O_{7-\delta}$ pyrochlore [288], and perovskite $La_{0.9}Sr_{0.1}Al_{0.65}Mg_{0.15}Fe_{0.20}O_{3-\delta}$ [89], and also by testing CH_4 oxidation over the catalysts comprising Cu, bimetallic Cu–Ni, and $Ce(Ln)O_{2-\delta}$ where Ln = Gd or Tb [289]. However, as Ni-ceria cermets suffer from the dimensional instabilities caused by the local $p(O_2)$ variations and minor TEC mismatch, the presence of one redox-stable phase with moderate thermal expansion, such as YSZ, is desirable to avoid the resultant increase of anodic polarization (inset in Fig. 14). The impact of ceria-based components increases with decreasing temperature [285] and becomes crucial under the IT SOFC operation conditions. An additional improvement can be achieved by the infiltration of nanocrystalline ceria onto the cermet anode surface (Fig. 16), enabling to enhance exchange rates for both solid electrolyte and electrode, to enlarge TPB and electrode surface area, to provide better contacts between the component particles, and even to increase tolerance towards sulfur poisoning [30, 259, 281, 285]. The effects of Ce^{3+} or Ce^{4+} presence in other oxide phases incorporated in the anode compositions, if any, are still not obvious. As an example, appraisal of $Zr_{0.57}Y_{0.15}Ce_{0.15}Ti_{0.13}O_{2-\delta}$ as an alternative anode material and as a component of Ni- and Cu-containing cermets demonstrated inferior electrochemical activity with respect to conventional Ni–YSZ [263]. Among the former cermets, the best performance at 773 K was observed for the electrode obtained by reduction of $CuO - Zr_{0.57}Y_{0.15}Ce_{0.15}Ti_{0.13}O_{2-\delta}$ (60–40 wt.%); heating above 873 K resulted in microstructural degradation [263]. In the case of $CeVO_4$-based additives, an alteration of electrocatalytic properties of the composite electrodes cannot be excluded, but the polarization was relatively high due to fast interaction between the cell materials [259].

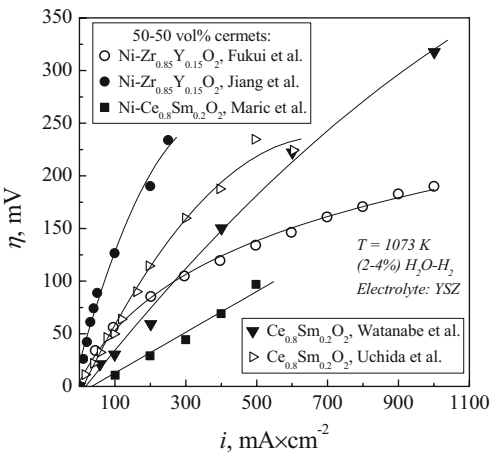

Fig. 15 Comparison of the anodic overpotentials of various zirconia- and ceria-based electrodes applied onto YSZ, in humidified hydrogen atmospheres [239, 279, 283, 345, 375]

Alternative oxide compositions and cermet components

The continuous search for alternative anode materials is primarily centered on perovskite-related structures, which are more tolerant to extensive cation substitution and possess better transport properties with respect to other families, such as spinels, fluorites, pyrochlores, C-type oxides, or garnets (e.g., [27, 71, 290–292]). Inspection of the low-$p(O_2)$ stability limits of the perovskite-related phases with a high electronic conduction and sufficient stability in oxidizing atmospheres as necessary for the fabrication and durable operation of SOFCs (Fig. 17) shows, however, that cobaltite-, manganite-, and ferrite-based compounds cannot be thermodynamically stable under anodic conditions. A variety of other compounds, such as rare-earth vanadates and molybdates, display attractive properties in reducing environments, but undergo phase changes leading to the formation of low-conductivity materials on oxidation [25, 287, 291–293]. The number of ternary oxide compounds which can be used as parent compositions for the anode developments is thus essentially limited, particularly to those in Cr- and Ti-containing systems.

One of the most known parent materials, $LaCrO_3$, is quite inert for the reactions associated with reforming and carbon deposition [294–298]. As for many other perovskites, the dominant *p*-type electronic conductivity and electrocatalytic activity of lanthanum chromite can be enhanced by the substitution of La^{3+} with alkaline-earth cations. At temperatures above 770 K, the methane oxidation and surface dissociation occur over $(La,A)CrO_{3-\delta}$ (A = Ca, Sr) anodes without significant coking [276, 298, 299], suggesting possible applications in hydrocarbon-fueled SOFCs. The electrochemical properties of chromites are however poor, a result of slow surface exchange, low total and ionic conductivities under anodic conditions, and often, weak adherence to the solid electrolyte ceramics. Very high polarization resistances are typical for most chromite-based compositions, in particular $La_{1-x}Sr_xCrO_{3-\delta}$ (x=0.2–0.3) and their derivatives, both in H_2–H_2O and CH_4–H_2O atmospheres even at elevated temperatures [23, 25, 298, 300–302]. The

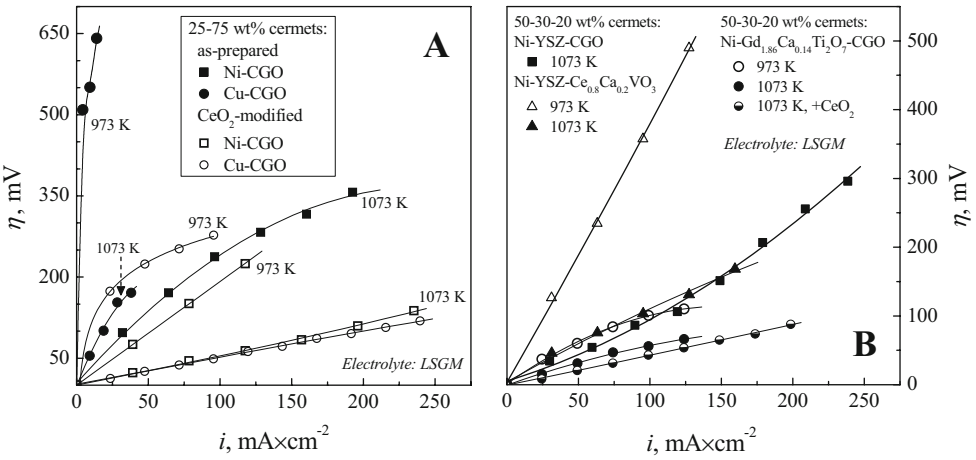

Fig. 16 **a**, **b** Overpotential vs. current density dependencies of Ce-containing cermet anodes in contact with $(La_{0.9}Sr_{0.1})_{0.98}Ga_{0.8}Mg_{0.2}O_{3-\delta}$ electrolyte, after preparation and after ceria infiltration onto the porous electrode [259, 285]

only known exceptions are related to the multiphase anodes where a highly dispersed catalyst is supported on porous chromite surface; examples include bimetallic Pd–Ni [303], or nickel formed on reduction of 10% Ni-substituted chromite solid solution [296]. Again, the overpotentials can be drastically decreased incorporating ceria additives. In the case of composite anodes obtained by reduction of $La_{0.8}Sr_{0.2}Cr_{0.98}V_{0.02}O_{3-\delta}$, $Ce_{0.9}Gd_{0.1}O_{2-\delta}$, and NiO (47.5:47.5:5 wt.%) in contact with $Ce_{0.9}Gd_{0.1}O_{2-\delta}$ electrolyte, the polarization resistance at 1023 K was as low as ~0.8 Ω cm^2 at 450 mV cell voltage and 0.1 Ω cm^2 under open-circuit conditions [304]. At the same time, systematic studies of $La_{1-x}A_xCr_{1-y}M_yO_{3-\delta}$ (M = Mg, Ti, Fe, V, Nb) perovskites [23, 295–299, 302, 305] did not reveal compositional domains with an appropriate combination of electrical, physicochemical, and catalytic properties, enabling to develop single-phase anode materials. For instance, the Cr-rich solid solutions possess a low electronic transport at reduced $p(O_2)$; the iron-containing materials suffer from an excessive chemically induced expansion and phase decomposition under anodic conditions, often stagnated owing to kinetic reasons [305]. As volume expansion on reduction may be suppressed by Ti doping [306], attention was attracted to $(La, A)(Cr, Ti)O_{3-\delta}$ electrodes, but their electrochemical performance is also insufficient for practical use [302].

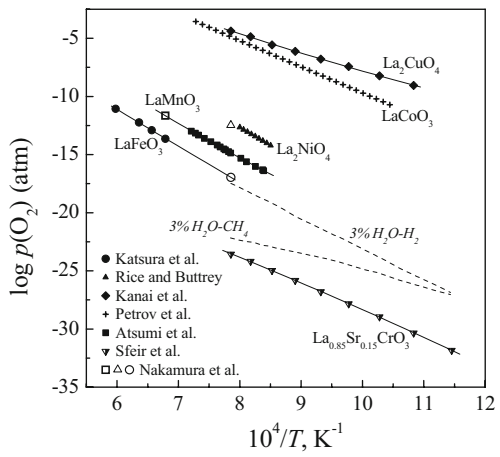

Fig. 17 Comparison of the low-$p(O_2)$ stability boundaries of perovskite-related oxide phases and oxygen chemical potentials typical for the SOFC anode environments [172, 305, 376–380]

On the contrary, promising properties were reported for perovskite-like $La_{1-x}Sr_xCr_{1-y}Mn_yO_{3-\delta}$ (x=0.2–0.3; $y\leq$0.5) and $Sr_2MoMg_{1-x}Mn_xO_{6-\delta}$ [291, 307–309], where the stabilization of oxygen-deficient lattices at low $p(O_2)$ becomes possible due to the presence of higher-valence cations retaining the neighboring oxygen polyhedra, while Mg^{2+} and Mn^{2+} cations are stable in both octahedral and tetrahedral coordination. Serious advantages of the former family (LSCM) include a substantial electrochemical activity in reducing and oxidizing atmospheres, compatibility with various solid electrolytes, and a good dimensional stability despite phase changes on reduction [307–316]. As an example, porous $La_{0.75}Sr_{0.25}Cr_{0.5}Mn_{0.5}O_{3-\delta}$ layers deposited onto YSZ and covered with Au paste and mesh, show anodic polarization resistances of 0.90 Ω cm^2 in diluted H_2 and 0.47 Ω cm^2 in wet 100% H_2 at 1198 K [307]. Low overpotentials were also observed for $(La_{0.75}Sr_{0.25})_{1-x}Cr_{0.5}Mn_{0.5}O_{3-\delta}$ (x=0–0.05) applied onto LSGM [312, 313, 315], and for $La_{0.8}Sr_{0.2}Cr_{0.8}Mn_{0.2}O_{3-\delta}$–Ni–$Ce_{0.9}Gd_{0.1}O_{2-\delta}$ cermets in contact with CGO [308]. Although a poor adherence was obtained for $La_{0.75}Sr_{0.25}Cr_{0.5}Mn_{0.5}O_{3-\delta}$ deposited onto zirconia, the electrochemical performance and adhesion both can be improved by YSZ additions [314], which also enhance ionic conduction in the anode materials. The ionic transport in LSCM is very low, in spite of the oxygen vacancy formation under reducing conditions (Fig. 18); consequently, CeO_2- and ZrO_2-based additives and interlayers decrease electrode polarization [307, 315–317]. The most crucial factor, relevant also for the majority of chromite- and titanate-based anodes, is however a relatively low electronic conduction. The total conductivity of LSCM lies in the range 20–40 S/cm and is essentially $p(O_2)$-independent in oxidizing and moderately reducing atmos-

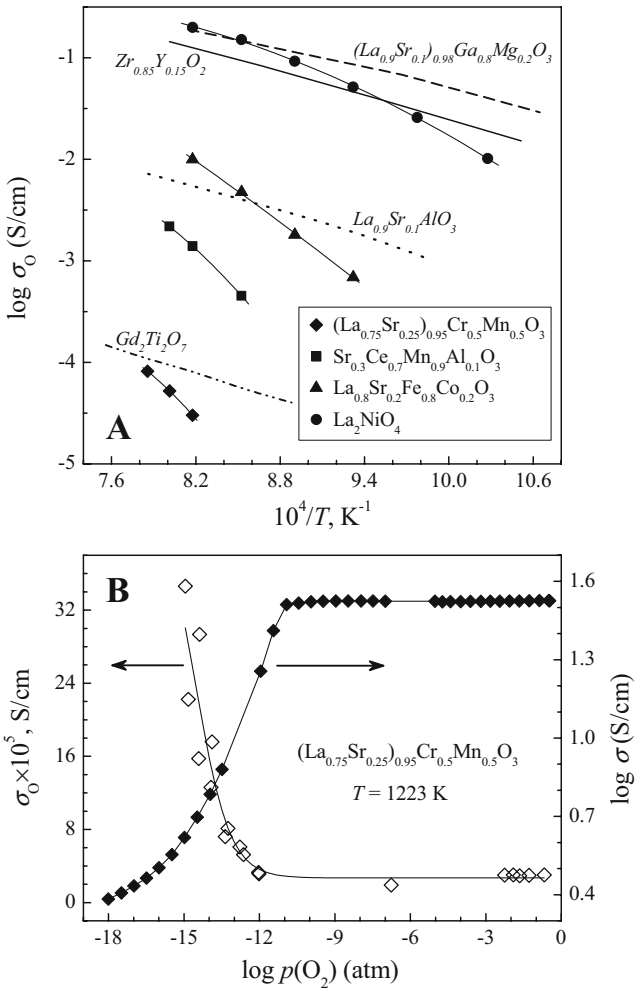

Fig. 18 Comparison of the partial oxygen ionic conductivities of selected mixed-conducting electrode materials [60, 101, 310, 381] and solid oxide electrolytes at oxygen partial pressures close to atmospheric (**a**), and oxygen pressure dependencies of the total and ionic conductivities of $(La_{0.75}Sr_{0.25})_{0.95}Cr_{0.5}Mn_{0.5}O_{3-\delta}$ [310] at 1223 K (**b**). The transport properties of solid electrolytes are discussed in the first part of this review

pheres at 1000–1250 K, but decreases down to 1–5 S/cm on reduction [307, 308, 310, 311]. Note that the current-constriction effects on electrode polarization, discussed in the first part of this review, are significant even for LSM where the conductivity is higher than 100 S/cm [318]. For model cells, the limiting effects of electronic transport can be avoided using specific current collectors, such as Au paste and mesh [307, 312, 313] or Ag paint [308]. This approach cannot be, however, used in real SOFCs; the practical current collectors made of stainless steels or $LaCrO_3$-based ceramics possess considerably higher contact and/or bulk resistances compared to the noble metals. The electronic transport limitations make it necessary to use LSCM in combination with metal additives, such as Ni or Cu [310, 315, 317], and to consider these phases among other promising components of the anode cermets.

Similar problems can be expected for $Sr_2Mo(Mg, Mn)O_{6-\delta}$ having a slightly higher total conductivity and, possibly, insufficient phase stability in reducing environments [291, 309, 319]. In the intermediate-temperature range, $Sr_2MoMgO_{6-\delta}$ may also suffer from the interaction with water vapor, SO_x or CO_2, as typical for the perovskites with large fractions of alkaline-earth cations in both sublattices (e.g., [320, 321]). Information on the behavior of LSCM and $Sr_2MoMg_{1-x}Mn_xO_{6-\delta}$ anodes in sulfur-containing atmospheres is still scarce [291, 316], though the latter system may be advantageous due to the catalytic activity of molybdenum species towards H_2S oxidation [322].

A higher *n*-type electronic conduction under reducing conditions is known for perovskite-related titanates [25, 27, 293, 297, 302, 323, 324]. However, the crystal and defect structure and transport properties of most conducting titanates stable in moderately reducing atmospheres tend to have an irreversible degradation on oxidation [323]. To some extent, this can be avoided by compositional optimization. For instance, the conductivity of 82 S/cm at 1073 K and $p(O_2)\approx 10^{-19}$ atm, structural stability over a wide range of temperatures and oxygen pressures, and thermal expansion compatible with solid oxide electrolytes were reported for $Sr_{0.86}Y_{0.08}TiO_{3-\delta}$ [324]. The typical polarization resistance, for $La_2Sr_4Ti_6O_{19}$ anodes at 1173 K, is 3.0 and 8.9 Ω cm^2 in wet H_2 and CH_4, respectively [325]. Such performance is yet insufficient, but enables to use titanate materials in the cermets.

Surface modification of solid electrolytes and electrodes

Regardless of the performance-determining role of electrode materials, the polarization losses in SOFCs can be significantly reduced altering composition and morphology of the solid electrolyte surface [13, 19–22, 326–335]. The exchange

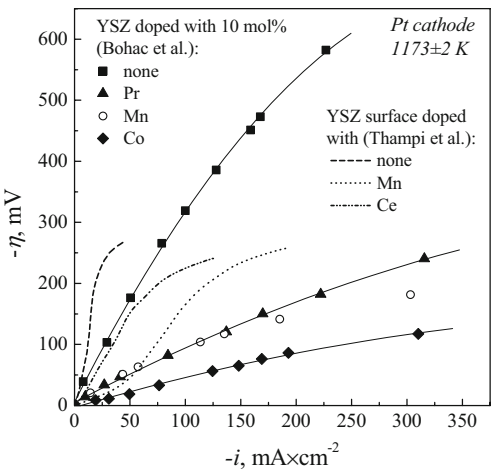

Fig. 19 Cathodic overpotentials of porous Pt electrodes in contact with YSZ electrolytes, bulk- [327] or surface- [336] doped with variable-valence cations

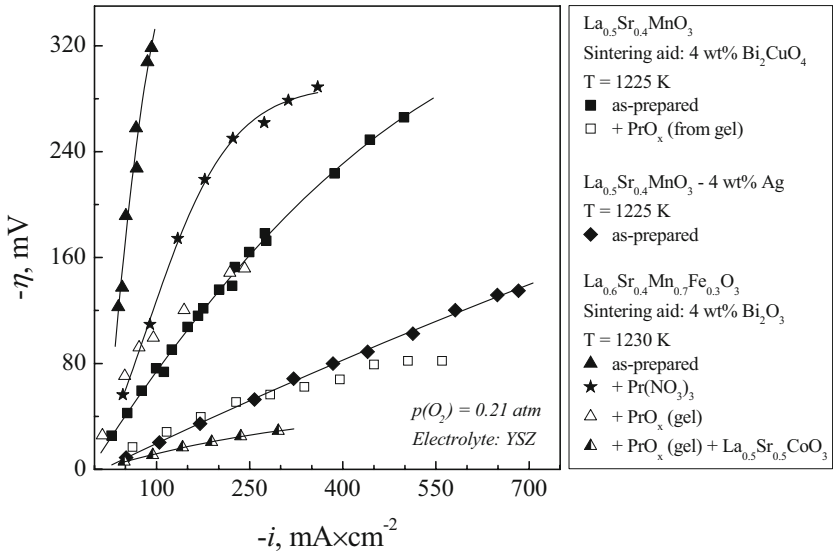

Fig. 20 Comparison of the overpotential vs. current dependencies for (La,Sr)(Mn,Fe)O_3 cathodes before and after surface modification [50, 357]

currents may be increased via the incorporation of variable-valence dopants with a high catalytic activity (Fig. 19), which participate in the electrode reaction, and via various chemical and physical treatments of the electrolyte surface in order to enhance specific area and electrode adhesion, to increase TPB length, and/or to remove ion transfer-blocking phases from the interface. Typical dopants include Ce, Ti, Mo, or Ni for the anode surface and Pr, Mn, Fe, or Co for the cathode; the relevant mechanisms are related to a local increase of the electronic transport, creation of the catalytic centers, inhibition of the blocking layer formation between the electrolyte and perovskite electrode, reducing grain-boundary resistance at the electrolyte surface, and scavenging of siliceous impurities [56, 326–328, 332, 333, 336–341]. The doping strategies should, however, account for possible diffusion into the electrolyte bulk and for redox changes in the surface layers during the cell operation in order to avoid excessive leakage currents and mechanical strains, which become critical in the IT SOFCs with thick film electrolytes. For the removal of siliceous phases from the electrolyte surface, chemical etching is usually considered as more effective and simpler method (e.g., [331]). Moreover, although the positive effects of surface doping with iron may partly result from the impurity-scavenging phenomena [340], data on the electrochemical behavior of Fe-doped YSZ ceramics and single crystals ([30, 328, 333, 337, 342] and references cited) require additional studies. In particular, the implantation of Fe^{3+} in the zirconia surface layer (~30 nm) has no essential influence on the oxygen reduction mechanisms, but leads to ten to 50 times higher exchange currents of porous Au electrodes at 770–1070 K [328, 337]; further heating causes iron dissolution in the YSZ bulk. Qualitatively similar improvements were achieved by forming cathodic sub-layers enriched with Pr or Mn, and by incorporating Ce or Ni in the anodic sub-layers, with the insertion depths varying from nano-scale up to a few microns [119, 326, 332, 333, 336]. It should be mentioned that Mn doping enables also to suppress zirconate formation at the LSM|YSZ interfaces [56], as for the use of Ln-site-deficient manganites. On the other hand, massive

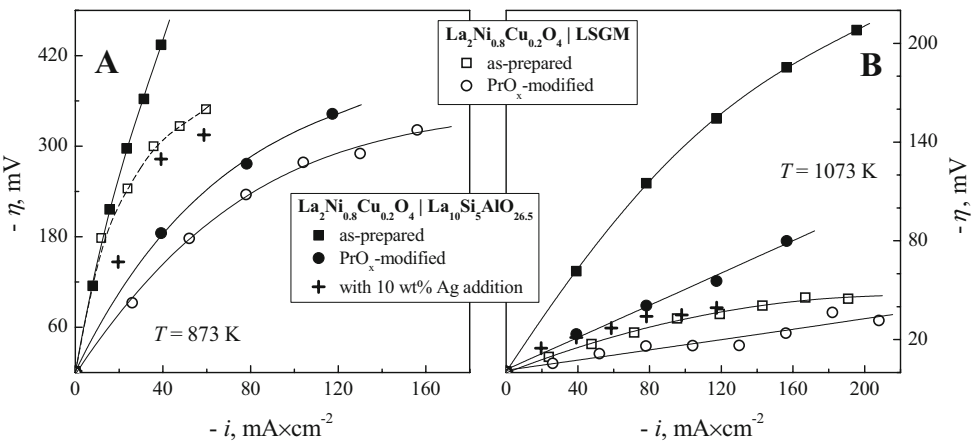

Fig. 21 **a**, **b** Cathodic overpotentials of porous $La_2Ni_{0.8}Cu_{0.2}O_{4+\delta}$ electrodes applied onto $La_{10}Si_5AlO_{26.5}$ and LSGM solid electrolytes with and without 10 wt.% Ag additions, before and after surface modification with praseodymia [270]

diffusion of the transition metal cations decreases ionic conductivity in most solid electrolytes, including ZrO_2-, CeO_2-, $LaGaO_3$-, Bi_2O_3-, and $La_{10}Si_6O_{27}$-based materials [32, 90, 158, 167, 186, 266, 343, 344]. This factor and the changes in electrode kinetics observed when the electrolyte surface layers contain large amounts of the variable-valence species (e.g., [259, 270, 310]) make it necessary to carefully control cation diffusion into solid electrolyte in the course of fuel cell fabrication if even no blocking interfacial layers can be formed.

The performance of SOFC electrodes can also be increased applying highly dispersed catalysts onto their surface, though the resultant effects cannot be usually separated from those associated with other factors, such as catalyst deposition onto the electrolyte and in the vicinity of TPB, increasing specific surface area, or reducing contact resistance and current-constriction effects. The catalytically active agents include, first of all, submicron- or nano-sized noble metal particles effective for most oxide and cermet electrodes [50, 122, 214, 283, 323, 345, 346]. Several examples illustrating the influence of silver additions, either introduced into the cathode composition prior to sintering or infiltrated into sintered porous layers via the impregnation with Ag-containing solutions, are given in Figs. 8a, 20, and 21. Note that, despite relatively high costs and potential instabilities [346, 347], silver incorporation is widely assessed for the IT SOFC electrodes [131, 270, 346, 348–353]; as a rule, the impacts are positive, though the electrochemical behavior is strongly dependent on the processing conditions governing Ag distribution in the porous electrodes and at the interface. For example, no essential catalytic effect was observed when introducing 0.1–2.0 wt.% Ag in $La_{0.65}Sr_{0.3}MnO_3$ cathodes synthesized by the Pechini method [349], in contradiction with other data [50, 119, 270, 310, 346]. Analogous discrepancies are well known for most catalysts where the activity is determined by submicron-scale morphology. In the case of minor additions of metallic nickel, significantly lower polarization was found for the anodes made of mixed-conducting $Ce_{0.6}Gd_{0.4}O_{2-\delta}$, $Ti_{0.22}Y_{0.16}Zr_{0.92}O_{2-\delta}$, $La_{0.75}Sr_{0.25}Cr_{0.97}V_{0.03}O_{3-\delta}$, and $(La_{0.75}Sr_{0.25})_{0.95}Cr_{0.5}Mn_{0.5}O_{3-\delta}$, and also for cermet 40 vol.% Ni–60% $Ce_{0.9}Gd_{0.1}O_{2-\delta}$ [310, 354]; the polarization resistance of Ni–$Zr_{0.92}Y_{0.16}O_{1.92}$ (40–60 vol.%) remained almost unchanged [354]. This type of behavior requires a careful analysis of all possible contributions to the electrode kinetics when using metal-containing pastes for current collection in the model cells with oxide electrodes, even in the case of gold. Taking into account the high catalytic activity of highly dispersed Au particles stabilized on oxide supports (e.g., [355, 356] and references cited), the effects of metal spreading into the porous electrode bulk cannot be a priori neglected.

The oxide-activating agents that can be applied onto the electrode surface in order to improve exchange kinetics are similar to those effective for the electrolyte surface doping and for engineering of the nanostructured composite electrodes, briefly discussed above. In particular, the typical electrocatalysts used since the 1960s [18, 19, 30, 343] are praseodymium oxide under oxidizing conditions (Figs. 8, 20, and 21) and ceria in reducing environments (Fig. 16). Another well-known approach is based on the deposition of oxide compositions, which have fast oxygen exchange rates and a limited compatibility with solid oxide electrolytes, onto a stable porous electrode matrix. For instance, the polarization resistance of LSM cathodes can be substantially decreased via the infiltration or screen-printing of perovskite-type $(Ln, Sr)CoO_{3-\delta}$ [357, 358]. As for the optimized composite electrodes, an increase in the electrochemical activity is often observed when applying nano-sized particles of ionic conductors, such as doped ceria and even YSZ [62, 279]; again, however, the nature of such phenomena is complex and may hardly be ascribed to any single stage of the electrode processes. Furthermore, while the use of nanocrystalline components offers serious advantages due to a reduced defect-formation energy and enlarged surface area [359–361], the pronounced tendencies to aggregation, passivation, and materials interaction characteristic of the nanostructured electrodes lead to another kind of limitations related not only to the maximum operation temperature, but also to uniform current and heat distribution in the solid oxide fuel cells.

References

1. Minh NQ, Takahashi T (1995) Science and technology of ceramic fuel cells. Elsevier, Amsterdam
2. Singhal SC (2000) Mater Res Soc Bull 25:16
3. Yamamoto O (2000) Electrochim Acta 45:2423
4. Steele BCH (2001) J Mater Sci 36:1053
5. Huijsmans JPP (2001) Curr Opin Solid State Mat Sci 5:317
6. Gorte RJ (2005) AIChE J 51:2377
7. De Bruijn F (2005) Green Chem 7:132
8. Kendall K (2005) Int Mater Rev 50:257
9. Sun C, Stimming U (2007) J Power Sources 171:247
10. La O' GJ, In HJ, Grumlin E, Barbastatsis G, Shao-Horn Y (2007) Int J Energy Res 31:548
11. Beckel D, Bieberle-Hütter A, Harvey A, Infortuna A, Muecke UP, Prestat M, Rupp JLM, Gauckler LJ (2007) J Power Sources 171:325
12. Lessing PA (2007) J Mater Sci 42:3465
13. McEvoy AJ, Rambert S, Widmer S (1996) Nanostructure, defect chemistry and operating protocols influence SOFC performance. In: Thorstensen, B (eds) Proc 2nd Eur Solid Oxide Fuel Cell Forum (Oslo, May 1996). vol. 1. European SOFC Forum, Oberrohrdorf, Switzerland, pp 599–606
14. Bronin DI, Kuzin BL, Yaroslavtsev IY, Bogdanovich NM (2006) J Solid State Electrochem 10:651
15. Lust E, Möller P, Kivi I, Nurk G, Kallip S (2005) J Solid State Electrochem 9:882
16. Horita T, Kishimoto H, Yamaji K, Xiong Y, Sakai N, Brito ME, Yokokawa H (2006) Solid State Ionics 177:1941
17. Dalslet B, Blennow P, Hendriksen PV, Bonanos N, Lybye D, Mogensen M (2006) J Solid State Electrochem 10:547

18. Etsell TH, Flengas SN (1970) Chem Rev 70:339
19. Chebotin VN, Perfiliev MV (1978) Electrochemistry of solid electrolytes. Technical Information Center, US Department of Energy, Oak Ridge
20. Kinoshita K (1992) Electrochemical oxygen technology. Wiley, New York
21. Bouwmeester HJM, Burgraaf AJ (1996) Dense ceramic membranes for oxygen separation. In: Burggraaf, AJ, Cot, L (eds) Fundamentals of inorganic membrane science and technology. Elsevier, Amsterdam, pp 435–528
22. Riess I, Schoonman J (1997) Electrodics. In: Gellings, PJ, Bouwmeester, HJM (eds) CRC handbook of solid state electrochemistry. CRC, Boca Raton, pp 269–294
23. Palguev SF, Gilderman VK, Zemtsov VI (1990) High-temperature oxide electronic conductors for electrochemical devices. Nauka, Moscow
24. Baker R, Guindet J, Kleitz M (1997) J Electrochem Soc 144:2427
25. Kharton VV, Yaremchenko AA, Naumovich EN (1999) J Solid State Electrochem 3:303
26. Adler SB (2004) Chem Rev 104:4791
27. Fergus JW (2006) Solid State Ionics 177:1529
28. Bove R, Ubertini S (2006) J Power Sources 159:543
29. Jiang SP (2007) J Solid State Electrochem 11:93
30. Kharton VV, Naumovich EN, Vecher AA (1999) J Solid State Electrochem 3:61
31. Blum L, Meulenberg WA, Nabielek H, Steinberger-Wilckens R (2005) Int J Appl Ceram Technol 2:482
32. Gaiduk YS, Kharton VV, Naumovich EN, Nikolaev AV, Samokhval VV (1994) Inorg Mater 30:1360
33. Takeda Y, Tu HY, Sakaki H, Watanabe S, Imanishi N, Yamamoto O, Phillipps MB, Sammes NM (1997) J Electrochem Soc 144:2810
34. Takeda Y, Sakaki Y, Ichikawa T, Imanishi N, Yamamoto O, Mori M, Abe T (1994) Solid State Ionics 72:257
35. Ishihara T, Kudo T, Matsuda H, Takita Y (1995) J Electrochem Soc 142:1519
36. Hashimoto S, Iwahara H (2000) J Electroceram 4:225
37. Huang X, Liu J, Lu Z, Liu W, Pei L, He T, Liu Z, Su W (2000) Solid State Ionics 130:195
38. Schachtner R, Ivers-Tiffée E, Weppner W, Männer R, Wersing W (1995) Ionics 1:63
39. Al Daroukh M, Vashook VV, Ullmann H, Tietz F, Arual Raj I (2003) Solid State Ionics 158:141
40. Siebert E, Hammouche A, Kleitz M (1995) Electrochim Acta 40:1741
41. Lee HY, Cho WS, Oh SM, Wiemhöfer H-D, Göpel W (1995) J Electrochem Soc 142:2659
42. Yasumoto K, Mori N, Mizusaki J, Tagawa H, Dokiya M (2001) J Electrochem Soc 148:A105
43. Sakaki Y, Takeda Y, Kato A, Imanishi N, Yamamoto O, Hattori M, Iio M, Esaki Y (1999) Solid State Ionics 118:187
44. Kharton VV, Nikolaev AV, Naumovich EN, Vecher AA (1995) Solid State Ionics 81:201
45. Huebner W, Reed DM, Anderson HU (1997) Structure–property relationships in solid oxide fuel cells. In: Stimming, U, Singhal, SC, Tagawa, H, Lehnert, W (eds) SOFC V. The Electrochemical Society, Pennington, NJ, pp 411–420
46. Rim H-R, Jeung S-K, Jung E, Lee J-S (1998) Mater Chem Phys 52:54
47. van Roosmalen JAM, Cordfunke EHP (1992) Solid State Ionics 52:303
48. van Heuveln FH, Bouwmeester HJM (1997) J Electrochem Soc 144:134
49. Kamata H, Hosaka A, Mizusaki J, Tagawa H (1998) Solid State Ionics 106:237
50. Tikhonovich VN, Kharton VV, Naumovich EN, Savitsky AA (1998) Solid State Ionics 106:197
51. Takeda Y, Kanno R, Noda M, Tomida Y, Yamamoto O (1987) J Electrochem Soc 134:2656
52. Pena MA, Fierro JLG (2001) Chem Rev 101:1981
53. Jiang SP (2003) J Power Sources 124:390
54. Mitterdorfer A, Gauckler LJ (1998) Solid State Ionics 111:185
55. Yokokawa H, Sakai N, Kawada T, Dokiya M (1993) Chemical thermodynamic stability of the interface. In: Badwal, SPS, Bannister, MJ, Hannink, RHJ (eds) Science and technology of Zirconia V. The Australian Ceramic Society, Technomic Publ, Melbourne, Australia, pp 752–763
56. Weber A, Männer R, Waser R, Ivers-Tiffée E (1996) Denki Kagaku 64:582
57. Caillol N, Pijolat M, Siebert E (2007) Appl Surf Sci 253:4641
58. Holc J, Kuščer D, Hrovat M, Bernik S, Kolar D (1997) Solid State Ionics 95:259
59. Phillipps MB, Sammes NM, Yamamoto O (1999) Solid State Ionics 123:131
60. Marozau IP, Kharton VV, Viskup AP, Frade JR, Samakhval VV (2006) J Eur Ceram Soc 26:1371
61. Barbucci A, Viviani M, Panizza M, Delucchi M, Cerisola G (2005) J Appl Electrochem 35:399
62. Leng YJ, Chan SH, Khor KA, Jiang SP (2006) J Solid State Electrochem 10:339
63. Godoi GS, de Souza DPF (2007) Mater Sci Eng B 140:90
64. Chen K, Lu Z, Ai N, Chen X, Hu J, Huang X, Su W (2007) J Power Sources 167:84
65. Kim J-H, Song R-H, Kim JH, Lim T-H, Sun Y-K, Shin D-R (2007) J Solid State Electrochem 11:1385
66. Hagiwara A, Hobara N, Takizawa K, Sato K, Abe H, Naito M (2007) Solid State Ionics 178:1123
67. Gong W, Gopalan S, Pal UB (2004) J Mater Eng Perform 13:274
68. Goodenough JB, Zhou J-S (2001) Transport properties. In: Goodenough, JB (eds) Localized to itinerant electronic transition in perovskite oxides. Springer, Berlin, pp 17–114
69. McCammon C (1996) Phase Transit 58:1
70. Oleynikov NN, Ketsko VA (2004) Russ J Inorg Chem 49:1
71. Gauckler LJ, Beckel D, Buergler BE, Jud E, Muecke UP, Prestat M, Rupp LJM, Richter J (2004) Chimia 58:837
72. Mai A, Haanappel VAC, Uhlenbruck S, Tietz F, Stöver D (2005) Solid State Ionics 176:1341
73. Lashtabeg A, Skinner SJ (2006) J Mater Chem 16:1
74. Liu Y, Tan X, Li K (2006) Catal Rev 48:145
75. Kharton VV, Yaremchenko AA, Shaula AL, Viskup AP, Marques FMB, Frade JR, Naumovich EN, Casanova JR, Marozau IP (2004) Defect Diffus Forum 226–228:141
76. Patrakeev MV, Leonidov IA, Kozhevnikov VL, Kharton VV (2004) Solid State Sci 6:907
77. Markov AA, Patrakeev MV, Kharton VV, Pivak YV, Leonidov IA, Kozhevnikov VL (2007) Chem Mater 19:3980
78. Kovalevsky AV, Kharton VV, Snijkers FMM, Cooymans JFC, Luyten JJ, Marques FMB (2007) J Membrane Sci 301:238
79. Patrakeev MV, Bahteeva JA, Mitberg EB, Leonidov IA, Kozhevnikov VL, Poeppelmeier KR (2003) J Solid State Chem 172:219
80. Tsipis EV, Patrakeev MV, Kharton VV, Yaremchenko AA, Mather GC, Shaula AL, Leonidov IA, Kozhevnikov VL, Frade JR (2005) Solid State Sci 7:355
81. Kharton VV, Patrakeev MV, Waerenborgh JC, Kovalevsky AV, Pivak YV, Gaczyński P, Markov AA, Yaremchenko AA (2007) J Phys Chem Solids 68:355
82. Jennings AJ, Skinner SJ, Helgason O (2003) J Solid State Chem 175:207
83. Lein HL, Wiik K, Grande T (2006) Solid State Ionics 177:1795
84. Søgaard M, Hendriksen PV, Mogensen M (2007) J Solid State Chem 180:1489
85. Zajac W, Swierczek K, Molenda J (2007) J Power Sources 173:675

86. Kharton VV, Yaremchenko AA, Patrakeev MV, Naumovich EN, Marques FMB (2003) J Eur Ceram Soc 23:1417
87. Kharton VV, Shaulo AL, Viskup AP, Avdeev M, Yaremchenko AA, Patrakeev MV, Kurbakov AI, Naumovich EN, Marques FMB (2002) Solid State Ionics 150:229
88. Park CY, Jacobson AJ (2005) Solid State Ionics 176:2671
89. Tsipis EV, Kharton VV, Vyshatko NP, Frade JR, Marques FMB (2005) Solid State Sci 7:257
90. Kharton VV, Figueiredo FM, Navarro L, Naumovich EN, Kovalevsky AV, Yaremchenko AA, Viskup AP, Carneiro A, Marques FMB, Frade JR (2001) J Mater Sci 36:1105
91. Kammer K, Mikkelsen L, Bilde-Sørensen JB (2006) J Solid State Electrochem 10:1432
92. Hashimoto S, Kammer K, Larsen PH, Poulsen FW, Mogensen M (2005) Solid State Ionics 176:1013
93. Prado F, Gurunathan K, Manthiram A (2002) J Mater Chem 12:2390
94. Shaula AL, Pivak YV, Waerenborgh JC, Gaczyński P, Yaremchenko AA, Kharton VV (2006) Solid State Ionics 177:2923
95. Kindermann L, Das D, Nickel H, Hilpert K (1996) Solid State Ionics 89:215
96. Kindermann L, Das D, Nickel H, Hilpert K, Appel CC, Poulsen FW (1997) J Electrochem Soc 144:717
97. Anderson MD, Stevenson JW, Simner SP (2004) J Power Sources 129:188
98. Kostogloudis GC, Tsiniarakis G, Ftikos C (2000) Solid State Ionics 135:529
99. Simner SP, Shelton JP, Anderson MD, Stevenson JW (2003) Solid State Ionics 161:11
100. Hrovat M, Holc J, Bernik S, Makovec D (1998) Mater Res Bull 33:1175
101. Kharton VV, Kovalevsky AV, Viskup AP, Shaula AL, Figueiredo FM, Naumovich EN, Marques FMB (2003) Solid State Ionics 160:247
102. Sakai N, Horita T, Yamaji K, Brito ME, Yokokawa H, Kawakami A, Matsuoka S, Watanabe N, Ueno A (2006) J Electrochem Soc 153:A621
103. Shaula AL, Kharton VV, Marques FMB (2004) J Eur Ceram Soc 24:2631
104. Shaula AL, Kharton VV, Marques FMB, Kovalevsky AV, Viskup AP, Naumovich EN (2006) J Solid State Electrochem 10:28
105. Sakai N, Kishimoto H, Yamaji K, Horita T, Brito ME, Yokokawa H (2007) J Electrochem Soc 154:B1331
106. Wan J-H, Yan J-Q, Goodenough JB (2005) J Electrochem Soc 152:A1511
107. Ullmann H, Trofimenko N, Tietz F, Stöver D, Ahmad-Khanlou A (2000) Solid State Ionics 138:79
108. Hayashi H, Suzuki M, Inaba H (2000) Solid State Ionics 128:131
109. Kostogloudis GC, Ftikos C (1999) Solid State Ionics 126:143
110. Riza F, Ftikos C, Tietz F, Fischer W (2001) J Eur Ceram Soc 21:1769
111. Jiang SP (2002) Solid State Ionics 146:1
112. Bae J-M, Steele BCH (1998) Solid State Ionics 106:247
113. Kostogloudis GC, Ftikos C, Ahmad-Khanlou A, Naoumidis A, Stöver D (2000) Solid State Ionics 134:127
114. Stevenson JW, Armstrong TR, Carneim RD, Pederson LR, Weber WJ (1996) J Electrochem Soc 143:2722
115. Petrov AN, Cherepanov VA, Zuev AYu (2006) J Solid State Electrochem 10:517
116. Huang K, Lee HY, Goodenough JB (1998) J Electrochem Soc 145:3220
117. Takeda Y, Ueno H, Imanishi N, Yamamoto O, Sammes N, Phillipps MB (1996) Solid State Ionics 86–88:1187
118. Lee HY, Oh SM, Seo IY, Rocholl F, Wiemhöfer HD (1997) The cathodic activity and interfacial stability of $Y_{0.8}Ca_{0.2}Co_{1-x}Fe_xO_3$/YSZ electrodes. In: Stimming, U, Singhal, SC, Tagawa, H, Lehnert, W (eds) SOFC V. The Electrochemical Society, Pennington, NJ, pp 520–529
119. Naumovich EN, Kharton VV, Samokhval VV, Kovalevsky AV (1997) Solid State Ionics 93:95
120. Ishihara T, Honda M, Shibayama T, Furutani H, Takita Y (1998) Ionics 4:395
121. Chen F, Xia C, Liu M (2001) Chem Lett 30:1032
122. Uchida H, Arisaka S, Watanabe M (2002) J Electrochem Soc 149:A13
123. Uhlenbruck S, Tietz F (2004) Mater Sci Eng B 107:277
124. Lust E, Möller P, Kivi I, Nurk G, Kallip S (2005) J Solid State Electrochem 9:882
125. Kharton VV, Tsipis EV, Yaremchenko AA, Marozau IP, Viskup AP, Frade JR, Naumovich EN (2006) Mater Sci Eng B 134:80
126. Taskin AA, Lavrov AN, Ando Y (2005) Appl Phys Lett 86:091910
127. Streule S, Podlesnyak A, Sheptyakov D, Pomyakushina E, Stingaciu M, Conder K, Medarde M, Patrakeev M, Leonidov I, Kozhevnikov V, Mesot J (2006) Phys Rev B 73:094203
128. Tarascon A, Skinner SJ, Chater RJ, Hernandez-Ramirez F, Kilner JA (2007) J Mater Chem 17:3175
129. Tarascon A, Morata A, Dezanneau G, Skinner SJ, Kilner JA, Estrade S, Hernandez-Ramirez F, Peiro F, Morante JR (2007) J Power Sources 174:255
130. Valldor M (2004) Solid State Sci 6:251
131. Tsipis EV, Kharton VV, Frade JR, Nunez P (2005) J Solid State Electrochem 9:547
132. Hao H, Cui J, Chen C, Pan L, Hu J, Hu X (2006) Solid State Ionics 177:631
133. Lee KT, Manthiram A (2006) Chem Mater 18:1621
134. Kawada T, Sase M, Kudo M, Yashiro K, Sato K, Mizusaki J, Sakai N, Horita T, Yamaji K, Yokokawa H (2006) Solid State Ionics 177:3081
135. Tsipis EV, Kharton VV, Frade JR (2006) Solid State Ionics 177:1823
136. Petric A, Huang P, Tietz F (2000) Solid State Ionics 135:719
137. Kharton VV, Naumovich EN, Vecher AA, Nikolaev AV (1995) J Solid State Chem 120:128
138. Ishihara T, Fukui S, Nishiguchi H, Takita Y (2002) Solid State Ionics 152–153:609
139. Ohbayashi H, Kudo T, Gejo T (1974) Jpn J Appl Phys 13:1
140. Kharton VV, Naumovich EN, Zhuk PP, Demin AK, Nikolaev AV (1992) Russ J Electrochem 28:1376
141. Morin F, Trudel G, Denos Y (1997) Solid State Ionics 96:129
142. Poznyak SK, Kharton VV, Frade JR, Yaremchenko AA, Tsipis EV, Yakovlev SO, Marozau IP (2008) J Solid State Electrochem 12:15
143. Bucher E, Sitte W, Rom I, Rapst I, Grogger W, Hofer F (2002) Solid State Ionics 152–153:417
144. van Doorn RHE, Burggraaf AJ (2000) Solid State Ionics 128:65
145. Svarcova S, Wiik K, Tolchard J, Bouwmeester HJM, Grande T (2008) Solid State Ionics 178:1787
146. Vente JF, McIntosh S, Haije WG, Bouwmeester HJM (2006) J Solid State Electrochem 10:581
147. Baumann FS, Fleig J, Cristiani G, Stuhlhofer B, Habermeier H-U, Maier J (2007) J Electrochem Soc 154:B931
148. Peña-Martinez J, Marrero-Lopez D, Perez-Coll D, Ruiz-Morales JC, Nuñez P (2007) Electrochim Acta 52:2950
149. Shao Z, Xiong G, Tong J, Dong H, Yang W (2001) Sep Purif Technol 25:419
150. Vente JF, Haije WG, Rak ZS (2006) J Membrane Sci 276:178
151. Zeng P, Chen Z, Zhou W, Gu H, Shao Z, Liu S (2007) J Membrane Sci 291:148
152. Fisher CAJ, Yoshiya M, Iwamoto Y, Ishii J, Asanuma M, Yabuta K (2007) Solid State Ionics 177:3425
153. Yan A, Cheng M, Dong Y, Yang W, Maragou V, Song S, Tsiarakas P (2006) Appl Catal B 66:64

154. Simner SP, Shelton JP, Anderson MD, Stevenson JW (2003) Solid State Ionics 161:11
155. Chen W, Wen T, Nie H, Zheng R (2003) Mater Res Bull 38:1319
156. Yokokawa H, Sakai N, Horita T, Yamaji K, Brito ME, Kishimoto H (2008) J Alloys Compd 452:41
157. Bronin DI, Kuzin BL, Sokolova YV, Polyakova NV (2000) Russ J Appl Chem 73:1557
158. Kharton VV, Naumovich EN, Yaremchenko AA, Marques FMB (2001) J Solid State Electrochem 5:160
159. Kuzin BL, Bogdanovich NM, Bronin DI, Yaroslavtsev IY, Vdovin GK, Kotov YA, Bagazeev AV, Medvedev AI, Murzakaev AM, Timoshenkova OP, Stolts AK (2007) Russ J Electrochem 43:920
160. Zhu XD, Sun KN, Zhang NQ, Chen XB, Wu LJ, Jia DC (2007) Electrochem Commun 9:431
161. Zhou W, Shao Z, Ran R, Chen Z, Zeng P, Gu H, Jin W, Xu N (2007) Electrochim Acta 52:6297
162. Serra JM, Vert VB, Betz M, Haanappel VAC, Meulenberg WA, Tietz F (2008) J Electrochem Soc 155:B207
163. Ishihara T, Honda M, Nishiguchi H, Takita Y (1997) Solid oxide fuel cell operable at decreased temperature using $LaGaO_3$ perovskite oxide electrolyte. In: Stimming, U, Singhal, SC, Tagawa, H, Lehnert, W (eds) SOFC V. The Electrochemical Society, Pennington, NJ, pp 301–310
164. Anderson HU (1992) Solid State Ionics 52:33
165. van Hassel BA, Kawada T, Sakai N, Yokokawa H, Dokiya M, Bouwmeester HJM (1993) Solid State Ionics 66:295
166. Tu HY, Takeda Y, Imanishi N, Yamamoto O (1999) Solid State Ionics 117:277
167. Kharton VV, Naumovich EN, Samokhval VV (1997) Solid State Ionics 99:269
168. Steele BCH (1995) Solid State Ionics 75:157
169. Endo A, Wada S, Wen C, Komiyama H, Yamada K (1998) J Electrochem Soc 145:L35
170. Fleig J (2002) J Power Sources 105:228
171. Fleig J, Maier J (2004) J Eur Ceram Soc 24:1343
172. Nakamura T, Petzow G, Gauckler LJ (1979) Mater Res Bull 14:649
173. Cheng J, Navrotsky A, Zhou XD, Anderson HU (2005) J Mater Res 20:191
174. Chiba R, Yoshimura F, Sakurai Y (1999) Solid State Ionics 124:281
175. Zinkevich M, Aldinger F (2004) J Alloys Compd 375:147
176. Bannikov DO, Cherepanov VA (2006) J Solid State Chem 179:2721
177. Amow G, Skinner SJ (2006) J Solid State Electrochem 10:538
178. Amow G, Davidson IJ, Skinner SJ (2006) Solid State Ionics 177:1205
179. Tsipis EV, Patrakeev MV, Waerenborgh JC, Pivak YV, Markov AA, Gaczyński P, Naumovich EN, Kharton VV (2007) J Solid State Chem 180:1902
180. Kovalevsky AV, Kharton VV, Yaremchenko AA, Pivak YV, Tsipis EV, Yakovlev SO, Markov AA, Naumovich EN, Frade JR (2007) J Electroceram 18:205
181. Gaiduk YS, Kharton VV, Naumovich EN, Samokhval VV (1994) Inorg Mater 30:759
182. Chiba R, Yoshimura F, Sakurai Y (2002) Solid State Ionics 152–153:575
183. Kiselev EA, Proskurnina NV, Voronin VI, Cherepanov VA (2007) Inorg Mater 43:167
184. Hashimoto S, Kammer K, Poulsen FW, Mogensen M (2007) J Alloys Compd 428:256
185. Kharton VV, Viskup AP, Naumovich EN, Tikhonovich VN (1999) Mater Res Bull 34:1311
186. Kharton VV, Viskup AP, Yaremchenko AA, Baker RT, Gharbage B, Mather GC, Figueiredo FM, Naumovich EN, Marques FMB (2000) Solid State Ionics 132:119
187. Yakovlev SO, Kharton VV, Naumovich EN, Zekonyte J, Zaporojtchenko V, Kovalevsky AV, Yaremchenko AA, Frade JR (2006) Solid State Sci 8:1302
188. Boehm E, Bassat J-M, Steil MC, Dordor P, Mauvy F, Grenier J-C (2003) Solid State Sci 5:973
189. Vashook V, Yushkevich I, Kokhanovsky L, Makhnach L, Tolochko S, Kononyuk I, Ullmann H, Altenburg H (1999) Solid State Ionics 119:23
190. Tsipis EV, Naumovich EN, Patrakeev MV, Waerenborgh JC, Pivak YV, Gaczyński P, Kharton VV (2007) J Phys Chem Solids 68:1443
191. Skinner SJ, Kilner JA (2000) Solid State Ionics 135:709
192. Kharton VV, Viskup AP, Kovalevsky AV, Naumovich EN, Marques FMB (2001) Solid State Ionics 143:337
193. Tsipis EV, Naumovich EN, Shaula AL, Patrakeev MV, Waerenborgh JC, Kharton VV (2007) Solid State Ionics 179:57
194. Mauvy F, Lalanne C, Bassat J-M, Grenier J-C, Zhao H, Dordor Ph, Stevens P (2005) J Eur Ceram Soc 25:2669
195. Kharton VV, Kovalevsky AV, Avdeev M, Tsipis EV, Patrakeev MV, Yaremchenko AA, Naumovich EN, Frade JR (2007) Chem Mater 19:2027
196. Kharton VV, Tsipis EV, Yaremchenko AA, Frade AA (2004) Solid State Ionics 166:327
197. Kim GT, Wang S, Jacobson AJ, Yuan Z, Chen C (2007) J Mater Chem 17:1316
198. Amow G, Whitfield PS, Davidson IJ, Hammond RP, Munnings CN, Skinner SJ (2004) Ceram Int 30:1635
199. Wan J, Goodenough JB, Zhu JH (2007) Solid State Ionics 178:281
200. Laberty C, Zhao F, Swider-Lyons KE, Virkar AV (2007) Electrochem Solid State Lett 10:B170
201. Schenck P (ed) (1998) Phase equilibria diagrams. CD-Rom database. The American Ceramic Society, Westerville, OH
202. Wong NGW, Cook LP (1992) AIChE Symp Ser 88:11
203. Osamura K, Zhang W (1993) Mater Res Adv Tech 84:522
204. Singh KK, Morris DE, Sinha APB (1994) Physica C 231:377
205. Kale GM, Kumar RV, Fray DJ (1996) Solid State Ionics 86–88:1421
206. Kononyuk IF, Tikhonova LA, Makhnach LV, Zhavnerko GK (1983) Neorg Mater 19:934
207. Berenov A, Wei J, Wood H, Rudkin R, Atkinson A (2007) J Solid State Electrochem 11:482
208. Bochkov DM, Kharton VV, Kovalevsky AV, Viskup AP, Naumovich EN (1999) Solid State Ionics 120:281
209. Opila EJ, Tuller HL, Wuensch BJ, Maier J (1993) J Am Ceram Soc 76:2363
210. Routbort JL, Rothman SJ, Flandermeyer BK, Nowicki LJ, Baker JE (1988) J Mater Res 3:116
211. Mazo GN, Savvin SN, Abakumov AM, Hadermann J, Dobrovol'skii Yu A, Leonova LS (2007) Russ J Electrochem 43:436
212. Patrakeev MV, Leonidov IA, Kozhevnikov VL, Tsidilkovskii VI, Demin AK, Nikolaev AV (1993) Solid State Ionics 66:61
213. Mozhaev AP, Mazo GN, Galkin AA, Khramova NV (1996) Russ J Inorg Chem 41:881
214. Chang CL, Lee TC, Huang TJ (1998) J Solid State Electrochem 2:291
215. Mizusaki J, Tagawa H, Katou M, Hirano K, Sawata A, Tsuneyoshi K (1991) Electrochemical properties of some perovskite-type oxides as oxygen gas electrodes on yttria stabilized zirconia. In: Grosz, F, Zegers, P, Singhal, SC, Yamamoto, O (eds) SOFC II. The Electrochemical Society, Pennington, NJ, pp 487–494
216. Li Q, Zhao H, Huo L, Sun L, Cheng X, Grenier J-C (2007) Electrochem Commun 9:1508
217. Murray EP, Barnett SA (2001) Solid State Ionics 143:265
218. Zhao H, Huo L, Gao S (2004) J Power Sources 125:149
219. Xia C, Rauch W, Chen F, Liu M (2002) Solid State Ionics 149:11

220. Hart NT, Brandon NP, Day MJ, Lapena-Rey N (2002) J Power Sources 106:42
221. Imahara K, Jacobson CP, Visco SJ, De Jonghe LC (2005) Solid State Ionics 176:451
222. Jiang SP (2006) Mater Sci Eng A 418:199
223. Wang W, Gross MD, Vohs JM, Gorte RJ (2007) J Electrochem Soc 154:B439
224. Sunde S (1995) J Electrochem Soc 142:L50
225. Kenjo T, Nishiya M (1992) Solid State Ionics 57:295
226. Wang S, Jiang Y, Zhang Y, Yan J, Li W (1998) J Electrochem Soc 145:1932
227. Kim JD, Kim GD, Moon JW, Lee HW, Lee KT, Kim CE (2000) Solid State Ionics 133:67
228. Jørgensen MJ, Primdahl S, Bagger C, Mogensen M (2001) Solid State Ionics 139:1
229. Murray E, Tsai T, Barnett S (2002) Solid State Ionics 110:235
230. Murray EP, Sever MJ, Barnett SA (2002) Solid State Ionics 148:27
231. Wang S, Kato T, Nagata S, Honda T, Kaneko T, Iwashita N, Dokiya M (2002) Solid State Ionics 146:203
232. Liu Y, Rauch W, Zha S, Liu M (2004) Solid State Ionics 166:261
233. Sarantaridis D, Atkinson A (2007) Fuel Cells 7:246
234. Iida T, Kawano M, Matsui T, Kikuchi R, Eguchi K (2007) J Electrochem Soc 154:B234
235. Li S, Wang S, Nie H, Wen TL (2007) J Solid State Electrochem 11:59
236. Jung GB, Lo KF, Chan SH (2007) J Solid State Electrochem 11:1435
237. van Berkel FPF, van Heuveln FH, Huijsmans JPP (1994) Solid State Ionics 72:240
238. Lee DS, Lee JH, Kim J, Lee HW, Song HS (2004) Solid State Ionics 166:13
239. Fukui T, Murata K, Ohara S, Abe H, Naito M, Nogi K (2004) J Power Sources 125:17
240. Schneider LCR, Martin CL, Bultel Y, Dessemond L, Bouvard D (2007) Electrochim Acta 52:3190
241. Kim SD, Moon H, Hyun SH, Moon J, Kim J, Lee HW (2007) Solid State Ionics 178:1304
242. Kong J, Sun K, Zhou D, Zhang N, Mu J, Qiao J (2007) J Power Sources 166:337
243. Sunde S (2000) J Electroceram 5:153
244. Sunde S (1997) Electrochim Acta 42:2637
245. Barfod R, Mogensen M, Klemensø T, Hagen A, Liu YL, Hendriksen PV (2007) J Electrochem Soc 154:B371
246. Sunde S (1996) J Electrochem Soc 143:1123
247. Aruna ST, Muthuraman M, Patil KC (1998) Solid State Ionics 111:45
248. Skarmoutsos D, Tsoga A, Naoumidis A, Nikolopoulos P (2000) Solid State Ionics 135:439
249. Anselmi-Tamburini U, Chiodelli G, Arimondi M, Maglia F, Spinolo G, Munir ZA (1998) Solid State Ionics 110:35
250. Corbin SF, Qiao X (2003) J Am Ceram Soc 86:401
251. Koide H, Someya Y, Yoshida T, Maruyama T (2000) Solid State Ionics 132:253
252. Simwonis D, Tietz F, Stöver D (2000) Solid State Ionics 132:241
253. Iwata T (1996) J Electrochem Soc 143:1521
254. Fouquet D, Müller AC, Weber A, Ivers-Tiffée E (2003) Ionics 8:103
255. Kim H, Liu C, Worrell WL, Vohs JM, Gorte RJ (2002) J Electrochem Soc 149:A247
256. Gorte RJ, Park S, Vohs JM, Wang C (2000) Adv Mater 12:1465
257. Sato K, Sakamaki K, Inoue Y (2000) Mater Trans JIM 41:1621
258. Laguna-Bercero MA, Larrea A, Penã JI, Merino RI, Orera VM (2005) J Eur Ceram Soc 25:1455
259. Tsipis EV, Kharton VV, Frade JR (2005) J Eur Ceram Soc 25:2623
260. Grgicak CM, Green RG, Giorgi JB (2006) J Mater Chem 16:885
261. Ishihara T, Shinagawa M, Kawakami A, Matsumoto H (2007) Mater Sci Forum 539–543:1350
262. Grgicak CM, Green RG, Giorgi JB (2008) J Power Sources 179:317
263. Ruiz-Morales JC, Nunez P, Buchanan R, Irvine JTS (2003) J Electrochem Soc 150:A1030
264. Huang P, Horky A, Petric A (1999) J Am Ceram Soc 82:2402
265. Huang K, Wan J-H, Goodenough JB (2001) J Electrochem Soc 148:A788
266. Kharton VV, Yaremchenko AA, Viskup AP, Mather GC, Naumovich EN, Marques F (2001) J Electroceram 7:57
267. Yokokawa H, Sakai N, Horita T, Yamaji K, Brito ME (2005) Electrochem 73:20
268. Naumovich EN, Kharton VV, Yaremchenko AA, Patrakeev MV, Kellerman DG, Logvinovich DI, Kozhevnikov VL (2006) Phys Rev B 74:064105
269. Brisse A, Sauvet A-L, Barthet C, Beaudet-Savignat S, Fouletier J (2006) Fuel Cells 6:59
270. Tsipis EV, Kharton VV, Frade JR (2007) Electrochim Acta 52:4428
271. Mori M, Hiei Y, Itoh H, Tompsett GA, Sammes NM (2003) Solid State Ionics 160:1
272. Skarmoutsos D, Tsoga A, Naoumidis A, Nikolopoulos P (2000) Solid State Ionics 135:439
273. Fagg DP, Feighery AJ, Irvine JTS (2003) J Solid State Chem 172:277
274. Mantzouris X, Zouvelou N, Haanappel VAC, Tietz F, Nikolopoulos P (2007) J Mater Sci 42:10152
275. Möbius H-H, Rohland B (1868) US Patent 3377203
276. Steele BCH (1999) Nature 400:619
277. Marina OA, Bagger C, Primdahl S, Mogensen M (1999) Solid State Ionics 123:199
278. Kharton VV, Naumovich EN, Tikhonovich VN, Bashmakov IA, Boginsky LS, Kovalevsky AV (1999) J Power Sources 79:242
279. Jiang SP, Duan YY, Love JG (2002) J Electrochem Soc 149: A1175
280. Tu H, Apfel H, Stimming U (2006) Fuel Cells 6:303
281. Kurokawa H, Sholklapper TZ, Jacobson CP, De Jonghe LC, Visco SJ (2007) Electrochem Solid State Lett 10:B135
282. Beresnev SM, Kuzin BL, Bronin DI (2007) Russ J Electrochem 43:883
283. Uchida H, Suzuki H, Watanabe M (1998) J Electrochem Soc 145:615
284. Ishihara T, Shibayama T, Nishiguchi H, Takita Y (2000) Solid State Ionics 132:209
285. Tsipis EV, Kharton VV, Bashmakov IA, Naumovich EN, Frade JR (2004) J Solid State Electrochem 8:674
286. Tsipis EV, Shlyakhtina AV, Shcherbakova LG, Kolbanev IV, Kharton VV, Vyshatko NP, Frade JR (2003) J Electroceram 10:153
287. Tsipis EV, Kharton VV, Vyshatko NP, Shaula AL, Frade JR (2003) J Solid State Chem 176:47
288. Kharton VV, Tsipis EV, Yaremchenko AA, Vyshatko NP, Shaula AL, Naumovich EN, Frade JR (2003) J Solid State Electrochem 7:468
289. Hornés A, Gamarra D, Munuera G, Conesa JC, Martínez-Arias A (2007) J Power Sources 169:9
290. Atkinson A, Barnett S, Gorte RJ, Irvine JTS, McEvoy AJ, Mogensen M, Singhal SC, Vohs J (2004) Nature Mater 3:17
291. Goodenough JB, Huang Y-H (2007) J Power Sources 173:1
292. Hui S, Petric A (2001) Solid State Ionics 143:275
293. Bazuev GV, Shveikin GP (1985) Complex oxides of elements with completing *d*- and *f*-shells. Nauka, Moscow
294. Vernoux P, Guindet J, Gehain E, Kleitz M (1997) Catalysts for continuous methane reforming in medium temperature SOFC. In: Stimming, U, Singhal, SC, Tagawa, H, Lehnert, W (eds) SOFC V. The Electrochemical Society, Pennington, NJ, pp 219–227
295. Vernoux P (1997) Ionics 3:270

296. Sfeir J, Buffat PA, Möckli P, Xanthopoulos N, Vasquez R, Mathieu HJ, Van herle J, Thampi KR (2001) J Catal 202:229
297. Vashook V, Vasylechko L, Zosel J, Müller R, Ahlborn E, Guth U (2004) Solid State Ionics 175:151
298. Georges S, Parrour G, Henault M, Fouletier J (2006) Solid State Ionics 177:2109
299. Baker RT, Metcalfe IS, Middleton PH, Steele BCH (1994) Solid State Ionics 72:328
300. Sauvet A-L, Guindet J, Fouletier J (1999) Ionics 5:150
301. Primdahl S, Hansen JR, Grahl-Madsen L, Larsen PH (2001) J Electrochem Soc 148:A74
302. Pudmich G, Boukamp BA, Gonzalez-Cuenca M, Jungen W, Zipprich W, Tietz F (2000) Solid State Ionics 135:433
303. Nabae Y, Yamanaka I, Takenaka S, Hatano M, Otsuka K (2005) Chem Lett 34:774
304. Madsen BD, Barnett SA (2007) J Electrochem Soc 154:B501
305. Sfeir J (2003) J Power Sources 118:276
306. Tietz F (1999) Ionics 5:129
307. Tao S, Irvine JTS (2004) J Electrochem Soc 151:A252
308. Liu J, Madsen B, Ji Z, Barnett S (2002) Electrochem Solid State Lett 5:A122
309. Huang Y-H, Dass RI, Denyszyn JC, Goodenough JB (2006) J Electrochem Soc 153:A1266
310. Kharton VV, Tsipis EV, Marozau IP, Viskup AP, Frade JR, Irvine JTS (2007) Solid State Ionics 178:101
311. Zha S, Tsang P, Cheng Z, Liu M (2005) J Solid State Chem 178:1844
312. Tao S, Irvine JTS, Kilner JA (2005) Adv Mater 17:1734
313. Peña-Martínez J, Marrero-López D, Ruiz-Morales JC, Savaniu C, Núñez P, Irvine JTS (2006) Chem Mater 18:1001
314. Jiang SP, Chen XJ, Chan SH, Kwok JT, Khor KA (2006) Solid State Ionics 177:149
315. Wan J, Zhu JH, Goodenough JB (2006) Solid State Ionics 177:1211
316. Chen XJ, Liu QL, Chan SH, Brandon NP, Khor KA (2007) J Electrochem Soc 154:B1206
317. Ruiz-Morales JC, Canalez-Vazquez J, Marrero-López D, Irvine JTS, Núñez P (2007) Electrochim Acta 52:7217
318. Sasaki K, Wurtz J-P, Gschwend R, Gödickemeier M, Gauckler LJ (1996) J Electrochem Soc 143:530
319. Bernuy-Lopez C, Allix M, Bridges CA, Claridge JB, Rosseinsky MJ (2007) Chem Mater 19:1035
320. Glöckner R, Neiman A, Larring Y, Norby T (1999) Solid State Ionics 125:369
321. Animitsa IE, Neiman AYA, Kochetova NA, Korona DV (2006) Russ J Electrochem 42:311
322. Zha S, Cheng Z, Liu M (2005) Electrochem Solid State Lett 8: A406
323. Jiang SP, Chan SH (2004) J Mater Sci 39:4405
324. Hui S, Petric A (2002) J Eur Ceram Soc 22:1673
325. Slater PR, Irvine JTS (1999) Solid State Ionics 124:61
326. Schouler EJL (1983) Solid State Ionics 9–10:945
327. Bohac P, Orliukas A, Gauckler L (1994) Lowering of the cathode overpotential of SOFC by electrolyte doping. In: Waser, R, Hoffmann, S, Bonnenberg, D, Hoffmann, Ch (eds) Electroceramics IV. vol. II. IWE, University of Technology, Augustinus Buchhandlung, Aachen, pp 771–780
328. van Hassel BA, Boukamp BA, Burggraaf AJ (1992) Solid State Ionics 51:161
329. Kurumchin EKh, Perfilyev MV (1990) Solid State Ionics 42:129
330. Juhl M, Primdahl S, Manon C, Mogensen M (1996) J Power Sources 61:173
331. Bae JM, Steele BCH (1998) Solid State Ionics 106:247
332. Kurumchin EKh (1998) Ionics 4:390
333. McEvoy AJ (2000) Solid State Ionics 135:331
334. Tomita A, Hibino T, Sano M (2005) Electrochem Solid State Lett 8:A333
335. Rose L, Kesler O, Tang Z, Burgess A (2007) J Power Sources 167:340
336. Thampi KR, McEvoy AJ, Van herle J (1995) J Electrochem Soc 142:506
337. Scholten D, Burggraaf AJ (1985) Solid State Ionics 16:147
338. Asano K, Iwahara H (1997) J Electrochem Soc 144:3125
339. Kharton VV, Viskup AP, Figueiredo FM, Naumovich EN, Shaulo AL, Marques FMB (2002) Mater Lett 53:160
340. de Ridder M, van Welzenis RG, Brongersma HH, Kreissig U (2003) Solid State Ionics 158:67
341. Fagg DP, Kharton VV, Frade JR (2004) J Solid State Electrochem 8:618
342. Fabry P, Kleitz M (1974) J Electroanal Chem 57:165
343. Kharton VV, Yaremchenko AA, Naumovich EN, Marques FMB (2000) J Solid State Electrochem 4:243
344. Kharton VV, Shaula AL, Patrakeev MV, Waerenborgh JC, Rojas DP, Vyshatko NP, Tsipis EV, Yaremchenko AA, Marques FMB (2004) J Electrochem Soc 151:A1236
345. Watanabe M, Uchida H, Shibata M, Mochizuki N, Amikura K (1994) J Electrochem Soc 141:342
346. Simner SP, Anderson MD, Templeton JW, Stevenson JW (2007) J Power Sources 168:236
347. Lu ZG, Zhu JH (2007) Electrochem Solid State Lett 10:B179
348. Rutenbeck D, Haanappel VAC, Uhlenbruck S, Tietz F, Vinke IC, Stöver D (2003) Noble metals in SOFC cathodes: processing and electrochemical performance. In: Singhal, SC, Dokiya, M (eds) SOFC-VIII. The Electrochemical Society, Pennington, NJ, pp 615–623
349. Uhlenbruck S, Tietz F, Haanappel VAC, Sebold D, Buchkremer HP, Stöver D (2004) J Solid State Electrochem 8:923
350. Sholklapper TZ, Radmilovich V, Jacobson CP, Visco SJ, De Jonghe LC (2008) J Power Sources 175:206
351. Datta P, Majewski P, Aldinger F (2008) Mater Chem Phys 107:370
352. Wang F-Y, Cheng S, Wan B-Z (2008) Catal Commun 9:1595
353. Rossmeisl J, Bessler WG (2008) Solid State Ionics 178:1694
354. Primdahl S, Mogensen M (2002) Solid State Ionics 152:597
355. Glaspell G, Hassan HMA, Elzatahry A, Abdalsayed V, El-Shall MS (2008) Top Catal 47:22
356. Llorca J, Casanovas A, Domingues M, Casanova I, Angurell I, Seco M, Rossell O (2008) J Nanopart Res 10:537
357. Tikhonovich VN, Kharton VV, Naumovich EN (1997) Inorg Mater 33:602
358. Sasaki K, Gödickemeier M, Bohac P, Orliukas A, Gauckler LJ (1993) Microstructure design of mixed-conducting solid oxide fuel cell cathodes. In: Biedermann P, Krahl-Urban B (eds) Proc 5th IEA Workshop on SOFC Materials, Process Engineering and Electrochemistry. Forschungszentrum Jülich, Germany, pp 187–196
359. Christie GM, van Berkel FPF (1996) Solid State Ionics 83:17
360. Tuller HL (2000) Solid State Ionics 131:143
361. Liu Y, Zha S, Liu M (2004) Chem Mater 16:3502
362. Aruna ST, Muthuraman M, Patil KC (1999) Solid State Ionics 120:275
363. Tikhonova LA (1991) PhD Thesis, Belarus State University, Minsk
364. Srilomsak S, Schilling D, Anderson HU (1989) Thermal expansion studies on cathode and interconnect oxides. In: Singhal, SC (eds) SOFC I. The Electrochemical Society, Pennington, NJ, pp 129–140
365. Tai LW, Nasrallah MM, Anderson HU, Sparlin DM, Sehlin SR (1995) Solid State Ionics 76:273
366. Tai LW, Nasrallah MM, Anderson HU, Sparlin DM, Sehlin SR (1995) Solid State Ionics 76:259
367. Yamamoto O, Takeda Y, Kanno R, Kojima T (1989) Stability of perovskite oxide electrode with stabilized zirconia. In: Singhal,

SC (eds) SOFC I. The Electrochemical Society, Pennington, NJ, pp 242–253
368. Dees DW, Claar TD, Easler TE, Fee DC, Mrazek FC (1987) J Electrochem Soc 134:2141
369. Chiba R, Yoshimura F, Sakurai Y (2002) Solid State Ionics 152–153:575
370. Yu HC, Zhao F, Virkar AV, Fung KZ (2005) J Power Sources 152:22
371. Jiang SP, Ramprakash Y (1999) Solid State Ionics 116:145
372. Holtappels P, de Haart LGJ, Stimming U (1999) J Electrochem Soc 146:1620
373. Primdahl S, Mogensen M (1997) J Electrochem Soc 144:3409
374. Zhang X, Ohara S, Maric R, Mukai K, Fukui T, Yoshida H, Nishimura M, Inagaki T, Miura K (1999) J Power Sources 83:170
375. Maric R, Ohara S, Fukui T, Inagaki T, Fujita J (1998) Electrochem Solid State Lett 1:201
376. Petrov AN, Cherepanov VA, Zuev AYu (1987) Z Fiz Khim 61:630
377. Katsura T, Kitayama K, Sugihara T, Kimizuka N (1975) Bull Chem Soc Jpn 48:1809
378. Rice DE, Buttrey DJ (1993) J Solid State Chem 105:197
379. Kanai H, Mizusaki J, Tagawa H, Hoshiyama S, Hirano K, Fujita K, Tezuka M, Hashimoto T (1997) J Solid State Chem 131:150
380. Atsumi T, Ohgushi T, Kamegashira N (1996) J Alloys Compd 238:35
381. Tsipis EV, Naumovich EN, Shaula AL, Patrakeev MV, Waerenborgh JC, Kharton VV (2008) Solid State Ionics 179:57